



Budapest University of Technology and Economics
Faculty of Electrical Engineering and Informatics
Department of Control Engineering and Information Technology

Geometric modelling of the human vertebral body for diagnostics purposes

Scientific Students' Association Report

Author:

Sándor Bazsó

Advisor:

Balázs István Benyó, Ph.D.

Ákos Szlávecz, Ph.D.

Árpád Viola, M.D., Ph.D.

2020

Contents

Kivonat	i
Abstract	ii
1 Introduction	1
2 Previous works and Medical background	4
2.1 Spinal column	5
2.1.1 Vertebra	6
2.1.2 Compression fracture	8
2.1.3 Treatment	8
3 Methods and Data	10
3.1 B-spline	10
3.2 Catmull-Rom spline	12
3.3 Curve for vertebra modelling	12
3.4 Analysed dataset	13
3.5 Verification metrics	15
3.6 Model fitting protocol	16
3.7 Verification process	18
4 Results	19
4.1 Developed geometric model	19
4.1.1 Interpolating model	19
4.1.2 Approximating model	21
4.2 Model verification results	26
4.3 Validation of the model for solving medical problems	26
4.4 Framework	29
5 Discussion	33

6 Conclusions	36
6.1 Further work	37
Acknowledgements	38
Bibliography	39

Kivonat

A gerinccsigolya kompressziós törése egyre gyakrabban előforduló betegség a fokozatosan öregedő európai társadalmakban, mivel az idős emberek nagy számban szenvednek a csontok elgyengülését előidéző csontritkulásban, amely növeli a csigolyatest sérülésének rizikóját. Több eljárás létezik a törött csigolyák kezelésére, melyek finomítása folyamatosan napirenden van. A különböző kezelések kvantitatív összehasonlításához szükség van a csigolya, ill. a csigolyatest pontos geometriai modelljére. A beavatkozások eredményének elemzésén felül egy adott beteg csigolyájának geometriai modellje akár közvetlenül felhasználható a diagnosztika és a beavatkozás javítására. Egy pontos modell lehetőséget ad a csigolya komplex paramétereinek mérésére, amely nehéz, ill. esetenként nem lehetséges a hagyományos orvosi képmegjelenítő rendszerekben. Egy megfelelően definiált geometriai modell megkönnyítheti, ill. lehetőséget adhat egyszerű távolság és szögmérések automatikus végrehajtására.

A bemutatott kutatás célja, egy olyan geometriai modell definiálása, amely egyszerűen összeregisztrálható egy orvosi képkalkoló módszerrel (pl.: CT) készített képpel és megfelel a klinikai követelményeknek. Munkánk eredményeként olyan geometriai modell született, amely alkalmas az összes gerinccsigolya modellezésére a nyaki 1-es csigolyától az ágyéki 5-ös csigolyáig és segítségével számos elemzési és diagnosztikai feladat könnyen elvégezhető. Az egyszerű felhasználás érdekében a modell megadása az orvosi képen szereplő csigolyatest két zárólemezen meghatározott anatómia pontok kijelölésével történik. A kihívást a geometriai modell definiálása, valamint a minimálisan szükséges anatómiai pontok számának meghatározása jelentette. Ezek mennyiségének növelésével a modell pontossága javítható, cserébe viszont a pontok kijelölése válik időigényes folyamattá. A későbbi feldolgozási lépések leegyszerűsítése érdekében, a geometriai modell egy standardizált reprezentációját vezettük be. A modell és a feldolgozási folyamat verifikálása egészséges gerinc ágyéki szakaszának modellezésével történt.

A dolgozat első fejezetében a csigolya modellezésében és a hozzá kapcsolódó képfeldolgozási módszerekben közelmúltban született eredmények kerülnek bemutatásra. Számos kutatás folyt ezen a területen, de egyik sem definiált egy általánosan alkalmazható geometriai modellt. A kutatások többnyire kis számú csigolyán kerültek megvalósításra, ill. a modellezésre használt környezet számos esetben limitációkat jelentett. A második fejezetben a csigolyatest geometriai modellje, és annak különböző verzióinak ismertetése szerepel, amely finomhangolása iteratív lépéseken keresztül került megvalósításra. Agilis kutatási módszert alkalmaztunk, ahol az orvosokkal folytatott gyakori konzultáció alapján történtek változtatások a modellen. A következő fejezet kitér a modell verifikációjára és a pontosságának kvantitatív meghatározására, továbbá ebben a fejezetben kerülnek ismertetésre az elért klinikai eredmények, ill. azok értékelése. A dolgozatot a kutatás eredményeinek összefoglalója, ill. a lehetséges további kutatási lépések zárják.

Abstract

Compression vertebral fracture is becoming increasingly frequent injury due to the aging European society. Elderly people frequently suffer from osteoporosis in which bone weakening increases the risk of vertebral injuries. There are several procedures to treat the fractured vertebra, that can be refined. The quantitative comparison of these interventions requires accurate geometric modeling of the vertebra, especially the vertebral body. A geometrical model customized to the individual patient could be used to improve the treatment procedure, as well. An accurate model would allow to measure complex parameters of the vertebral body, that is infeasible or impractical with traditional medical image visualization systems. A geometrical model could even simplify and automate basic distance and angle measurements.

The goal of this study was to create a precise geometrical model which can be co-registered with a medical image (e.g. CT) and meet all the clinical requirements. The geometrical model have to be suitable to represent every vertebra in the spinal column from the first cervical to the fifth lumbar vertebra. For ease of use the model is suggested by marking anatomical points of the vertebral body's end plate on the medical image. The challenge was to determine the appropriate geometry of the model and the minimum number of required anatomical points. Increasing the count of these markers will improve the precision of the model, but in exchange the process of marking these points will become time consuming. To simplify the subsequent analysis steps, a standard representation of the geometrical model of the vertebral body was introduced. The model and processing workflow was verified in a study on the lumbar section of healthy spinal column.

In the first chapter of this paper will introduce the recent results on modeling and image processing of the vertebral body. There are number of studies in this field, but none of them provided a generally applicable model. Moreover these studies were mainly done on small number of vertebrae and they were limited by the modeling framework. In the second chapter of the study the final geometrical model, including the versions of this model, that was refined in iterative steps will be presented. An agile research methodology was applied, as we had to frequently consult with doctors and modify the model according to their feedback. Next chapter will deal with the verification of the model and quantitatively assessment it's accuracy. This section will also introduce clinical learning achieved using the geometrical model. In the final part of the paper we will discuss the results and summarize the conclusions.

Chapter 1

Introduction

With the advance of 3D medical imaging technologies, such as CT (Computer Tomography) and MRI (Magnetic Resonance Imaging), it became possible to model the organs of the human body without the need for an invasive medical procedure. These models can be used for measurements, prosthetic design or even the simulation of complex surgeries. This paper deals with geometric modelling of vertebrae and spinal column allowing morphological analysis and diagnostic decision support. Although it is possible to make simple measurements with traditional medical image visualization systems, the calculation of complex parameters, such as volume, surface, angle etc., and the comparison of distinct anatomical structures are often impossible or extremely time consuming. The field of vertebra modelling is an extensively researched area with several articles about the topic [1–20]. The majority of these studies aims to provide a highly accurate model of the given vertebra in a form of a mesh, typically a triangular mesh. This process gives a precise representation of the actual vertebra, however, it does not provide a geometrical description of it. Compared to a 3D mesh, it is significantly easier to make an analysis with a geometrical model. In addition, it is still possible to generate a mesh from the geometrical representation if necessary. Moreover, the articles in this topic focus on a specific vertebra or spine, thus, considering all these shortcomings, our research interest is focused on providing a generally applicable geometric model. To analyse the entire spine it is necessary to model not only the individual vertebra but also their relative position to each other. By using relative positions the scope of the study can be expanded from individual vertebra parameters to parameters of the spinal column, e.g. different distances and angles of the spine. Examples for the anatomical parameters used for describing the spine morphology are shown in Figure 1.1.

The goal of our research presented in this study, was to create a patient specific geometric model of the vertebral body and develop optimization methods to increase its accuracy. This would enable complex measurements and calculations on the specific patient's vertebrae and spinal column. The model has to be sufficiently robust to accurately represent healthy vertebrae in any section of the human spinal column. One of the key requirements was the capability to co-register the model with a 3D medical image, i.e. CT or MRI. The benefit of this is an easier process of model creation as the model can be visualized simultaneously with the 3D medical image, thus making the whole process more user friendly. Another advantage of this approach would be the capability to make hybrid measurements using the medical image and the model, i.e. marking measurement's one point on the medical image and the other on the model. In this paper healthy vertebrae were modelled and analysed in order to verify the model, but with minor modifications the model can be adapted to injured or fractured vertebrae. It is important to note that our

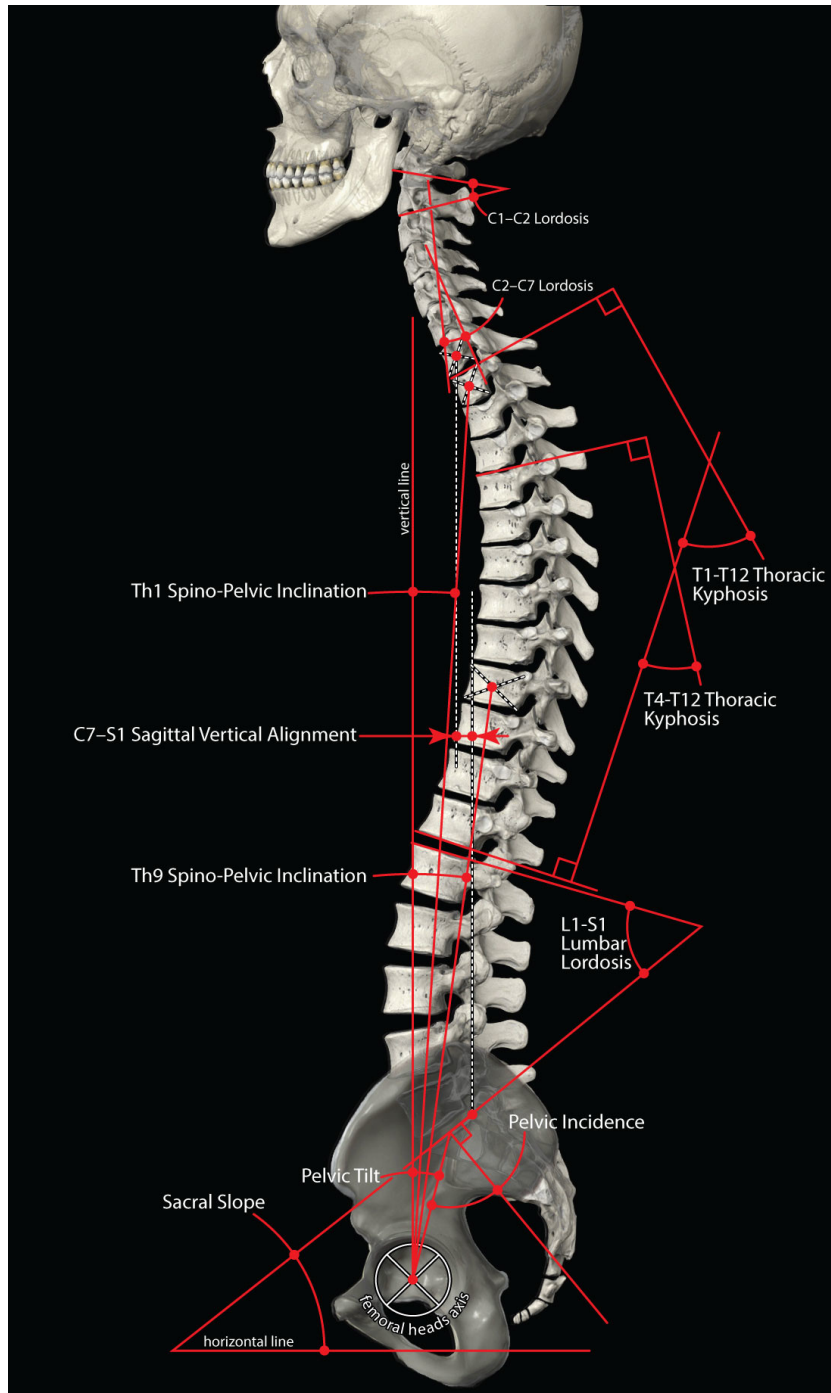


Figure 1.1: Typical distances and angles of the vertebral column analysed by medical doctors
(by Anatomy Standard[21] can be reused under the CC BY-NC 4.0[22])

aim was not to create the most accurate model of the vertebral body, rather, we aimed for a model that is easily and quickly applicable in exchange for some minor loss of accuracy. As a result of our research a novel geometric model is defined. This parametric model can be easily adjusted by marking certain anatomical points to create a patient specific model of the vertebral body.

To solve our research problem we have created a modelling environment to simultaneously visualize the model and the medical image. This framework was originally developed for cardiac simulations and modelling. To better match the purpose of this research some features were added to it. The two most notable ones are:

1. Capability to support multiple models to simplify comparison during the development process of the model.
2. Feature to rotate the slices of the medical image which optimizes the process of model fitting.

Apart from these, numerous improvements have been done to make the application more efficient and user friendly. Using this framework, the model can be adapted with relative ease to the individual vertebra. The core structure of the geometrical model has been created using B-splines. To minimize the error of surface fitting a parameter optimization method has been developed and implemented.

In the following chapter a brief introduction will be given on the anatomy of the human spinal column and its fundamental building blocks, the vertebrae. A possible application for the geometrical model will be presented, where a medical procedure could be improved using it. An overview will be provided on the articles dealing with the vertebra modelling and image processing. The 3rd chapter presents a detailed overview of the methods used for creating the geometrical model. This chapter also presents the process of validation and the dataset used for that. The 4th chapter describes the process of the development along with some challenges needed to be resolved to reach the desired outcome. The exact usage of the geometrical model will also be presented along with the model verification results. The validation of the model for solving medical problems will also be discussed. Finally, this chapter gives a short presentation of the most important features of the framework. Chapter 5 discusses the achieved results and the applicability of the framework. The 6th and final chapter summarizes the most important findings.

Chapter 2

Previous works and Medical background

The vast majority of the researches in this field focus on the segmentation of the vertebrae [1–20]. They propose a fully- or semi-automatic method with little to no human interaction [1–3, 10, 12, 13, 17, 18]. With the advance of artificial intelligence and the more readily available computational power necessary for their application, the segmentation process could be enhanced or even done entirely with CNNs (Convolutional Neural Network) [18]. In these studies AI is often utilized to further refine the segmentation. Some articles stop at this point and evaluate the quality of the segmentation by comparing the result with a golden reference. Usually these references are hand made segmentation of the vertebra by medical professionals. In other cases further processing steps are implemented [4–8, 11, 13]. A mesh, typically a triangular mesh, is fitted on the surface of the vertebra [4–7, 13] (see Figure 2.1). This allows the application of a finite element method for various analysis, for example the simulation of bone remodelling [6].

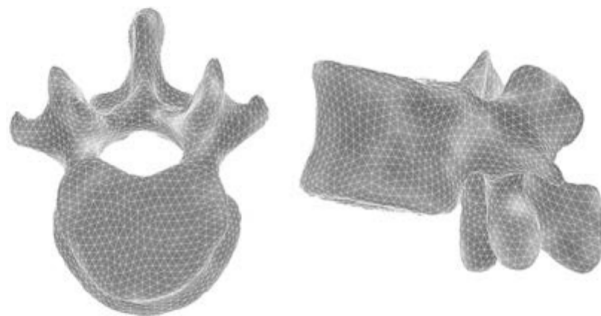


Figure 2.1: Mesh of a vertebra segmented by a semi automatic image processing method[13]

Most of these research are done on limited number of vertebra [2–4, 7, 8, 12, 12, 15, 15]. This could be a restricting factor for some studies, for example in the analysis of extreme parameters of the vertebra or rarely occurring anomalies. Other problem’s could raise from this, when AI is used and trained on a small dataset [18].

Usually the goal of these studies are to measure a specific vertebra parameter and make statistical analysis based on the examined patients [8, 13, 16]. The purpose of this paper is to provide a model that can be applied to individual person’s spinal column and make a patient specific model. This would allow the measurement of simple distance and angles showed on Figure 1.1, while adding the capability to compute complex parameters too,

such as volume or surface of the vertebral body or the cross section of the spinal canal. The generalisation of vertebrae modelling is a difficult task because they have complex anatomical structure and great variety in shape.

There is another perspective to take into consideration with these mesh based approach. If the automatic process fails somewhere either caused by the artefacts or noise on the image, insufficient spacial resolution or because a traumatic injury distorted the vertebra, the manual modification of these models could be difficult. We proposed a solution where the model fitting is done by medical professionals manually by placing markers on the image. This method also allows the utilization of automated steps in the workflow, thus creating a semi-automatic process. This way the possibility to easily make manual correction remains, while decreasing the amount of time required to fit the model.

It is not uncommon to use splines given by mathematical functions to describe anatomical structures in the human body [23–27]. They are often used for shape recognition or contour detection, which could be beneficial in a segmentation workflow. Other typical application is in the field of computer simulations, when a geometrical model’s behaviour is analysed in different scenarios. The mathematical description allows to precisely replicate different tissue’s size, shape, elasticity, strength, etc. under different circumstances.

2.1 Spinal column

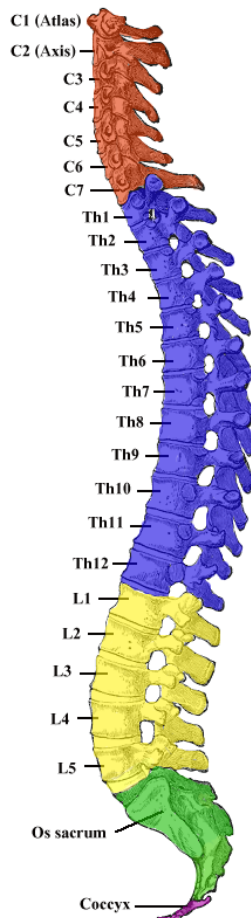


Figure 2.2: Human spine’s 5 section

The spinal column or vertebral column is part of the skeleton. It has two major roles in the human body. It is responsible to support the entire upper body, which includes the rib cage, head and upper limbs. The spinal cord, a key component of the central nervous system, runs in the well protected spinal canal. A rigid spinal column could be ideal for these purposes, but that would immobilize the entire axial skeleton. Therefore the vertebral column is made out of separate vertebrae which are articulated. Despite that some sections are fused to provide more rigidity. All in all this construct allows some movement but also provides good support and protection.

The spinal column can be divided into 5 sections (see Figure 2.2):

1. Cervical: 7 separated vertebrae (C1-C7)
2. Thoracic: 12 separated vertebrae (Th1-Th12)
3. Lumbar: 5 separated vertebrae (L1-L5)
4. Sacrum: 5 fused vertebrae (*Os sacrum*)
5. Coccyx (or tailbone): 3-5 fused vertebrae (*Coccyx*)

2.1.1 Vertebra

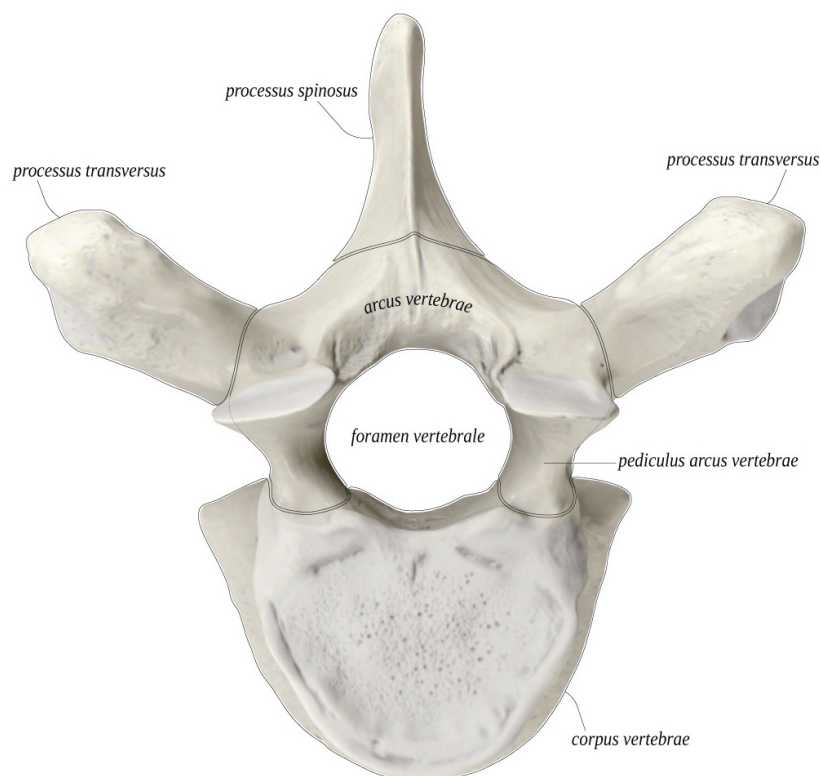


Figure 2.3: Typical vertebra's parts showed on a Th4
(by Anatomy Standard[21] can be reused under the CC BY-NC 4.0[22])

The shape and size of the vertebra varies between each part of the spine, but the main structure remains the same. Figure 2.3 shows a typical 4th thoracic vertebra and Figure 2.4 shows a 5th thoracic vertebra. The *vertebral foramen* (*foramen vertebrale*), where the

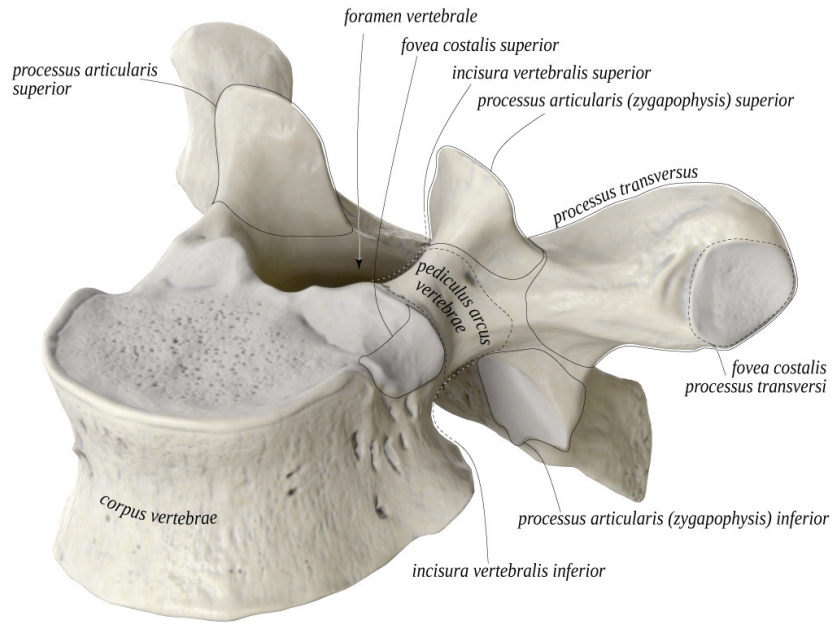


Figure 2.4: Typical vertebra's parts showed on a Th5
 (by Anatomy Standard[21] can be reused under the CC BY-NC 4.0[22])

spinal cord runs, is located at the centre of the vertebra. The *vertebral body* (*corpus vertebrae*) is found ventral from this. It is the main weight bearing component in the vertebra. Between two adjacent vertebral body there is a joint called *intervertebral disc* (*discus intervertebralis*), which allows slight movements of the vertebrae. On the dorsal side of the vertebra there are 4 *articular processes* (*processus articularis*), which allows the interlocking of the neighbouring vertebrae, thus preventing them from sliding on top of each other, which would damage the spinal cord. The *transverse process* (*processus transversus*) and *spinous process* (*processus spinosus*) serve as muscle attachment point for the muscles and articulation points for the rib cage.

In Figure 2.5 a comparison between the cervical, thoracic and lumbar vertebra is shown demonstrating the highly variable structure of the vertebra causing challenges in geometric modelling. From cervical toward lumbar part the size of the *vertebral body* increases as the load on the structure become greater. Same trend can be examined when looking at the processus of the vertebra.



Figure 2.5: Cervical (left), thoracic (middle), lumbar (right) vertebra
 (by Anatomy Standard[21] can be reused under the CC BY-NC 4.0[22])

2.1.2 Compression fracture

Compression fracture [28] [29] is a type of injury when the *vertebral body* collapses and therefore decreasing its height. It is often accompanied by heavy pain.

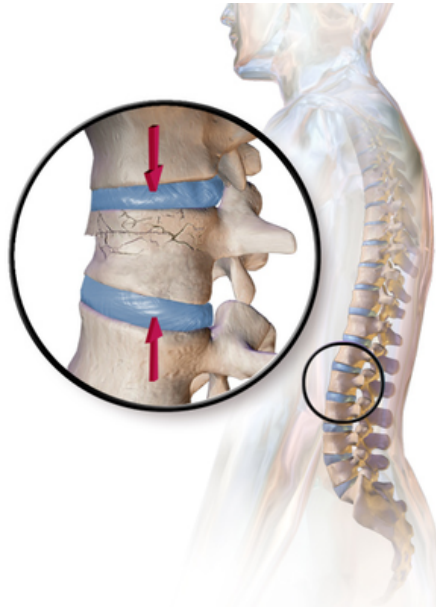


Figure 2.6: Illustration of the vertebra compression fracture
(by Bruce Blaus can be reused under the CC BY 3.0[30])

Osteoporosis is the leading cause of compression fracture. It is a bone weakening disease which mainly affects elderly people. As a result bones would break under minimal stress, such as lifting lighter objects or in extreme cases when someone sneeze. The disease affects women more frequently [31], but elderly men also suffer from it.

Severe trauma could lead to compression fracture of the vertebra in healthy people too. Car accident or falling in a way that the spinal column bends forward while being compressed are two prime cases of such accidents.

The third most frequent cause for compression fracture is related to metastatic tumours originated from cancer spread in the body. These tumours could weaken the bone and therefore the vertebral body collapses under little trauma.

2.1.3 Treatment

There are several treatment options for compressed vertebra, some does not require surgical intervention. In this paper our goal was to demonstrate a method for modelling the vertebral body which is relevant for the surgical treatment, therefore this method is briefly here.

The procedure is performed under local or general anaesthesia. A small incision is made on the back of the patient at the treated vertebra's height. Then with the help of an X-Ray machine a needle is guided into the vertebral body. The needle is used to fill the vertebral body with bone cement thus stabilizing the fractured vertebra.

An observation shows that more bone cement can be injected into the vertebral body if the vertebra is filled with saline solution before injecting the cement, thus increasing the

chance for successful therapy. A schematic comparison is shown on Figure 2.7. However, there is no easy and quantitative method to test this theory and quantitatively prove this observation because the same vertebra cannot be filled with cement two times. Moreover, there is a huge variety in size of the vertebral body between different patients and various part's of the spinal column. Therefore, in order to quantitatively compare the two procedures it is necessary to create a geometrical model of the vertebral body which would allow the estimation of the vertebral body's original volume by calculating the two neighbouring vertebral body's volume and extrapolating from those.

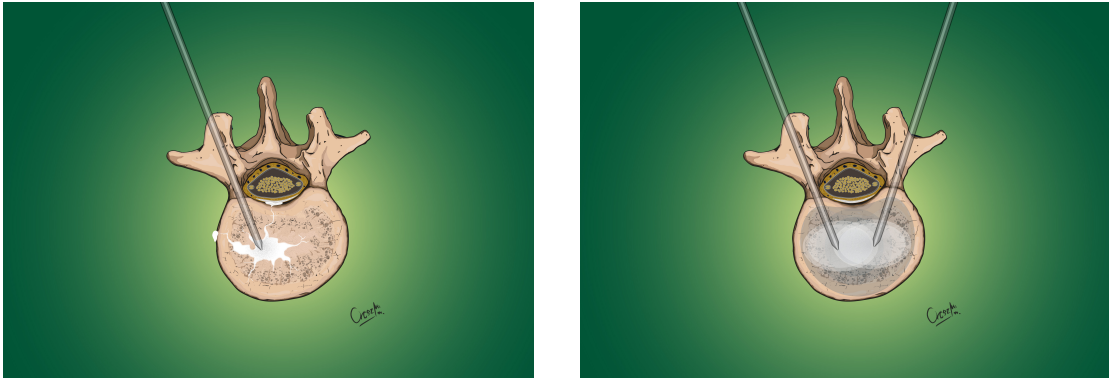


Figure 2.7: illustration of using only cement (left) or cement and saline solution (right)

Chapter 3

Methods and Data

Curves are continuous lines in the space [32], typically described by a mathematical expression, where the solution of the expression defines the points of the curve in an n^{th} dimensional (usually 3D) space. In practical applications the curves are often defined with so-called control points associated with certain part of the curve and basis functions describing the exact path of the curve on the given segment. The points of the curve are calculated by incrementing the t input parameter of the basis function. We can use weights to define the control's scope of the control points. Applying t dependent weights of the control points we can ensure several continuity features of the curve. There are two types of basis functions:

- interpolating and
- approximating

basis function. The fundamental difference is whether the curve passes through each control points or just approach them. In the interpolating case there is a t_k value of t parameter for each control points where weight 1 is associated to the k control point and 0 to every other. In the approximating case there is no such condition.

The most simple type of curve is a polyline. The control points are connected with a continuous straight lines. It has sharp edges, which means it is not continuously differentiable. These type of curves are frequently referred to as C^0 .

Bézier curve is an approximating type curve, which only intersects the first and last control points. It is a C^2 type, which means it is a twice continuously differentiable curve. One disadvantage of the Bézier curve is its global control, meaning changing one control point changes the slope of the whole curve.

3.1 B-spline

B-spline is an approximating type of curve. The control points, knots and the degree of the spline unambiguously identifies it. The curve runs inside the convex shell of the polygon defined by the control points, which means the control points will determinate the path of the curve. A B-spline is a piecewise polynomial with a given degree. The parts are separated with knots on the curve. In case of a first or higher degree B-spline the curve is approximated between neighbouring control points, therefore creating a continuous line. Increasing the degree of the spline will create a more smooth curve. A first degree B-spline

will approximate with a straight line, a second degree will produce a continuously differentiable curve, while a third degree B-spline will create a twice continuously differentiable curve (see Figure 3.1). One of the advantage of B-spline is the local control over the curve, which means changing one control point will only modify the surrounding part of the curve while leaving the rest in place. Increasing the degree of the curve means that more control points take place in the definition of a single point on the curve. In practice it means that increasing the degree of the polynomial expression will lessen the local control. On the other hand moving two neighbouring knots toward each other will cause the curve to move closer to the specific control point, thus approximating it better.

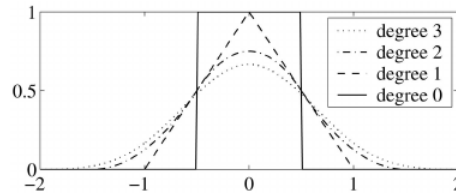


Figure 3.1: Degree of B-spline basis function from zero to three[33]

B-splines are widely used curves in different fields of industry. They can be used for drawing animated cartoon characters or rendering fonts. There is a broad spectrum of engineering applications too. From trajectory calculations for aircraft to modelling in the field of product design. Significant number of CAD (Computer Aided Design) software use B-spline for curved surfaces. The two major benefits over other curves are:

- smooth curve,
- local control.

The base plate of the vertebral body has a smooth outline without sharp edges, thus making it suitable to track with a B-spline. Figure 2.3 shows a typical thoracic vertebral body's base plate and Figure 3.2 a lumbar one. This feature of the vertebra and the versatility of B-splines makes this type of spline is suitable for vertebra modelling.



Figure 3.2: Vertebra base plate of a typical L3 vertebra
(by Anatomy Standard[21] can be reused under the CC BY-NC 4.0[22])

3.2 Catmull-Rom spline

In contrast with the B-spline, Catmull-Rom spline is an interpolating type curve. The tangent (v_k) in each control point is defined by the following expression:

$$v_k = \frac{p_{k+1} - p_{k-1}}{t_{k+1} - t_{k-1}}$$

where p_k is a control point and t_k is a knot. The Catmull-Rom spline is a piecewise third degree polynomial curve. It has a C^1 continuity, which means it's a continuously differentiable curve. When different derivatives are allowed at the two sides of a control point the continuity of the curve drops to C^0 . This construct provides a local control over the curve, meaning changing one control point only alters the surroundings of the given point.

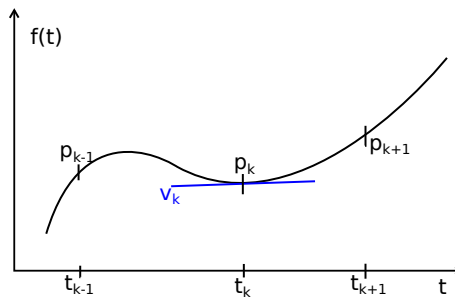


Figure 3.3: Catmull-Rom spline with tangent (v_k) at the p_k point

3.3 Curve for vertebra modelling

The vertebra body modelling requires a closed curve, a loop to represent the base plate of a vertebral body. This can be achieved differently with each type of spline. In order to create a closed curve from an open b-spline with $n + 1$ control points (P_0, P_1, \dots, P_n) and p degree another control point has to be added ($P_{n+1} = P_0$). Moreover $p + 2$ knots has to be added, which overlap with the first $p + 2$ knots ($u_{n+1} = u_0, u_{n+2} = u_1, \dots, u_{n+p+1} = u_p$). The closed curve's has C^{p-1} continuity at the joining point. A Catmull-Rom spline with $n + 1$ control points can be converted into a closed one, by adding a new control point the same way. If the two derivatives in this point equal the continuity of the curve will be C^1 .

Both Catmull-Rom and B-spline are suitable to model a vertebral body's shape, the exact implementation could be decided in favour of one to another.

In order to visualize the model described with splines, a mesh has to be created. By evaluating the spline at point t the coordinate of that point can be acquired in 3D space. Incrementing t parameter with a predefined size will generate points on the curve. Joining these points with a straight line will provide a polyline representation of the original spline. By lowering the step size in the previous step a more accurate representation of the spline can be made.

3.4 Analysed dataset

The two most frequently used medical imaging technologies that provide 3D anatomical structure of the human body are (see Figure 3.4)

- CT: Computer Tomography, and
- MRI: Magnetic Resonance Imaging.

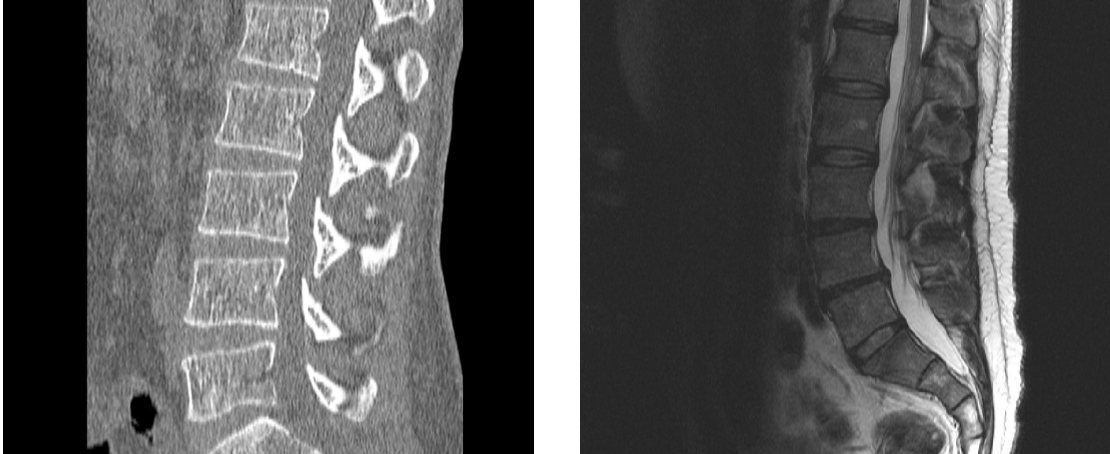


Figure 3.4: A sagittal slice of a CT (left) and MRI (right) showing a section of the spine
by gruntzooki is licenced under CC BY-SA 2.0[34]

There is a fundamental difference in the principals of CT and MRI imaging. CT machine calculates the voxel data from summational X-Ray images taken from different angles. Since X-Rays are attenuated more by dense tissues, for example bones than by soft tissue, this modality displays the skeleton with better contrast than it shows the internal organs. To standardize the CT images, a quantitative scale was introduced, called Hounsfield scale. Certain tissues are represented with a specific Hounsfield unit as shown on Figure 3.5. In this way unifying images of different vendor's machine and simplifying the interpretation of the data. On the other hand the MRI machine measures magnetic resonance. The human body is largely composed of water molecules. In each molecule there are two hydrogen atoms. MRI excites the hydrogen atoms with a large magnetic field and measures the radiation emitted by these excited atoms. Therefore it creates with higher contrast image where water is present in higher concentration. In practice this means the MRI creates a more detailed image of the soft tissue, and the skeleton is not visible. Both images can be enhanced with the use of contrast material to highlight parts relevant for the examination.

To validate our model we selected the lumbar segment of the vertebral column. The vertebrae of this part of the spine shows greater consistency in size and shape compared to the cervical section. Thoracic part would have meet this criteria as well but it has 12 vertebrae compared to the 5 of the lumbar section, that would have required more labour work to fit the model. CT is preferred over MRI, as it provides richer contrast when displaying bones. The third requirement toward the dataset: an available mask for the vertebrae to use as ground truth in the validation process.

We used a segmented lumbar vertebra CT database from the *University of Ljubljana, Faculty of Electrical Engineering, Laboratory of Imaging Technologies* [8][13]. This database

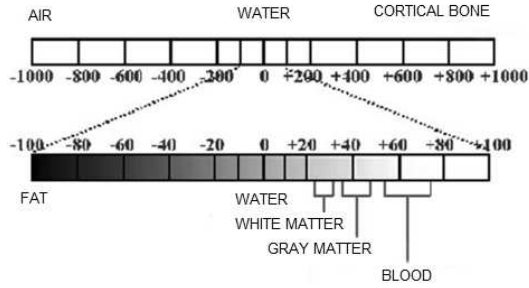


Figure 3.5: Hounsfield scale from -1000 to 1000 highlighting the typical values of different tissues [35]

contains 10 CT image of patients’ lumbar section of the vertebral column, with each vertebra hand segmented in it. This database was selected because it fulfils the above-mentioned three requirements (CT image, lumbar section, available mask).

Table 3.1 shows the technical parameters of the images in the database. Spacing shows the voxels’ distance from each other, while the resolution gives the number of voxels in each dimension.

The database contains 7 male and 3 female subject’s CT image, with mean age of 46 years, and 13.5 years standard deviation. 4 out of 10 patients has a healthy lumbar spine, we selected those for the modelling and analysis.

Image	Spac. S [mm]	Spac. C [mm]	Spac. A [mm]	Res. S	Res. C	Res. A
Subject01	0.28	0.28	1.07	1024	1024	200
Subject02	0.33	0.33	0.91	1024	1024	219
Subject03	0.34	0.34	0.81	1024	1024	260
Subject04	0.33	0.33	1.00	1024	1024	200
Subject05	0.37	0.37	1.28	1024	1024	200
Subject06	0.41	0.41	1.53	1024	1024	200
Subject07	0.33	0.33	0.97	1024	1024	240
Subject08	0.49	0.49	1.00	1024	1024	218
Subject09	0.45	0.45	1.13	1024	1024	270
Subject10	0.79	0.79	0.73	512	512	323

Table 3.1: Image technical parameters in the database (S - Sagittal, C - Coronal, A -Axial)

The images and the mask of the individual vertebrae are stored in a so called nearly raw raster data format (*.nrrd). This file format has two parts. A header where the most necessary metadata of the image is stored (spacing of the voxel, resolution, etc.), and a data section which can be compressed.

The modelling framework used in this study only supports DICOM (Digital Imaging and Communications in Medicine) format. This file type is developed for storing and transmitting medical images. Nowadays most of the scanners, workstations and visualisation software support this format. It has a rich metadata header which stores detailed information about the image, scanner, patient and the type of the examination. It has a wide range of supported modalities from radiography, ultrasonography, CT, and MRI.

In order to load the *.nrrd format images into the framework they need to be converted into DICOM format. The conversation was done in 3D Slicer, which is an open source flexible

and modular platform for medical image processing and analysis. It has a rich toolset for handling various image formats, advanced visualization features, segmentation and more. 3D Slicer were used for converting the images from *.nrrd format to DICOM and applying a transformation. Later was necessary to rotate the image into the traditional orientation, where the top of the axial view shows the anterior of the patient, the left side corresponds to the right side of the patient. In coronal view the head is towards the top of image, and the patient's left side is on the right. In sagittal view the head is towards the top of the image and the left side of it correspond to the anterior direction (see Figure 3.6). Finally, an offset had to be applied on the data to represent a Hounsfield scale.

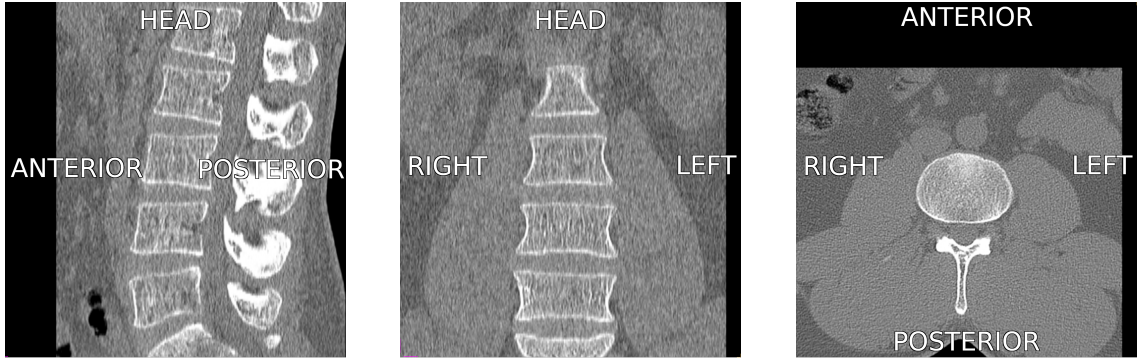


Figure 3.6: CT directions: Sagittal (left), Coronal (middle), Axial (right)

3.5 Verification metrics

In order to quantify the precision of the model similarity metrics were evaluated. These metrics give a numerical value representing the accuracy of the model based on given aspects.

Hausdorff metric is commonly called Hausdorff distance as its output can be interpreted as some sort of distance between the two compared sets. We evaluated the following 3 metrics related to Hausdorff distance:

- Hausdorff maximum distance ($d_H(X, Y)$): The maximum distance for all points in X, to the closest point in Y and vice versa. Formal mathematical expression:

$$d_H(X, Y) = \max \left\{ \max_{x \in X} \min_{y \in Y} d(x, y), \max_{y \in Y} \min_{x \in X} d(x, y) \right\}$$

- Hausdorff average distance ($d_{H,avg}(X, Y)$): The average distance for all points in X, to the closest point in Y and vice versa. Formal mathematical expression:

$$d_{H,avg}(X, Y) = \frac{1}{2} \cdot \left(\frac{1}{|X|} \sum_{x \in X} \min_{y \in Y} d(x, y) + \frac{1}{|Y|} \sum_{y \in Y} \min_{x \in X} d(x, y) \right)$$

- 95% Hausdorff distance: Similar to maximum Hausdorff distance, but the top 5% discarded, thus eliminating any error from a small set of outliers.

Dice coefficient is another typical metric for evaluating two sets similarity. 5 metrics were calculated:

1. Dice coefficient: Measures the overlap between the two sets (X and Y). Can be calculated with the following formula:

$$Dice = \frac{2|X \cap Y|}{|X| + |Y|}$$

where \cap represents the intersection and $+$ represents the union.

2. True positive (%): In the model the given voxel is correctly part of the vertebral body.
3. True negative (%): In the model the given voxel is correctly not part of the vertebral body.
4. False positive (%): In the model the given voxel is incorrectly marked as part of the vertebral body.
5. False negative (%): In the model the given voxel is incorrectly marked as not part of the vertebral body.

3.6 Model fitting protocol

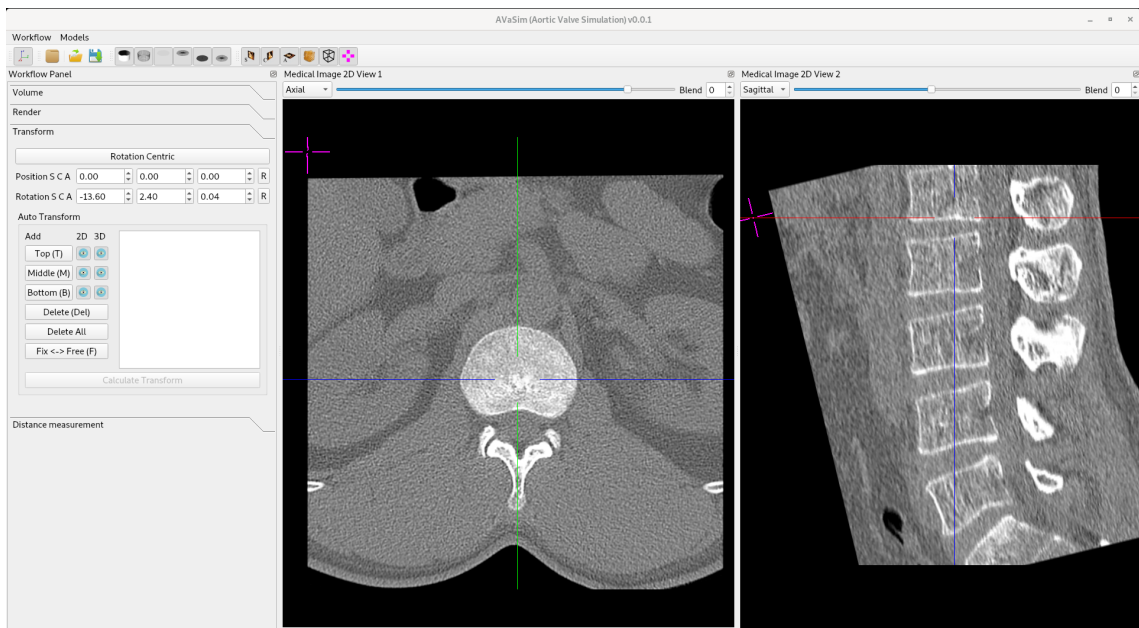


Figure 3.7: Model fitting: 2D view aligned to the vertebral body's base plate

The medical professional goes through the following steps defined in the model fitting protocol to fit the model (see Figure 3.8):

1. Load the DICOM image into the framework.
2. Move between the slices in the 2D view to reach the desired vertebra. In this process the guidelines, showing the other 2D view's position, help the user to navigate in the 3D space and identify the correct vertebra.

3. In a delicate process the 2D image is rotated to line up with the base plate of the vertebral body (see Figure 3.7).
4. The marking of the base plate's contour begins with the 4 fixed points on the axis. The frameworks automatically denotes the first 4 points as fixed points, therefore no user intervention required in order to correctly mark these significant points.
5. Mark the remaining points.
6. Step 2-5. then repeated for the other base plate of the vertebra and for a middle plane between the two base plates. Figure 4.6 shows the 3 planes where the landmark placement is done.
7. Model calculation based on the marked points.
8. Finally the model is labelled and saved.

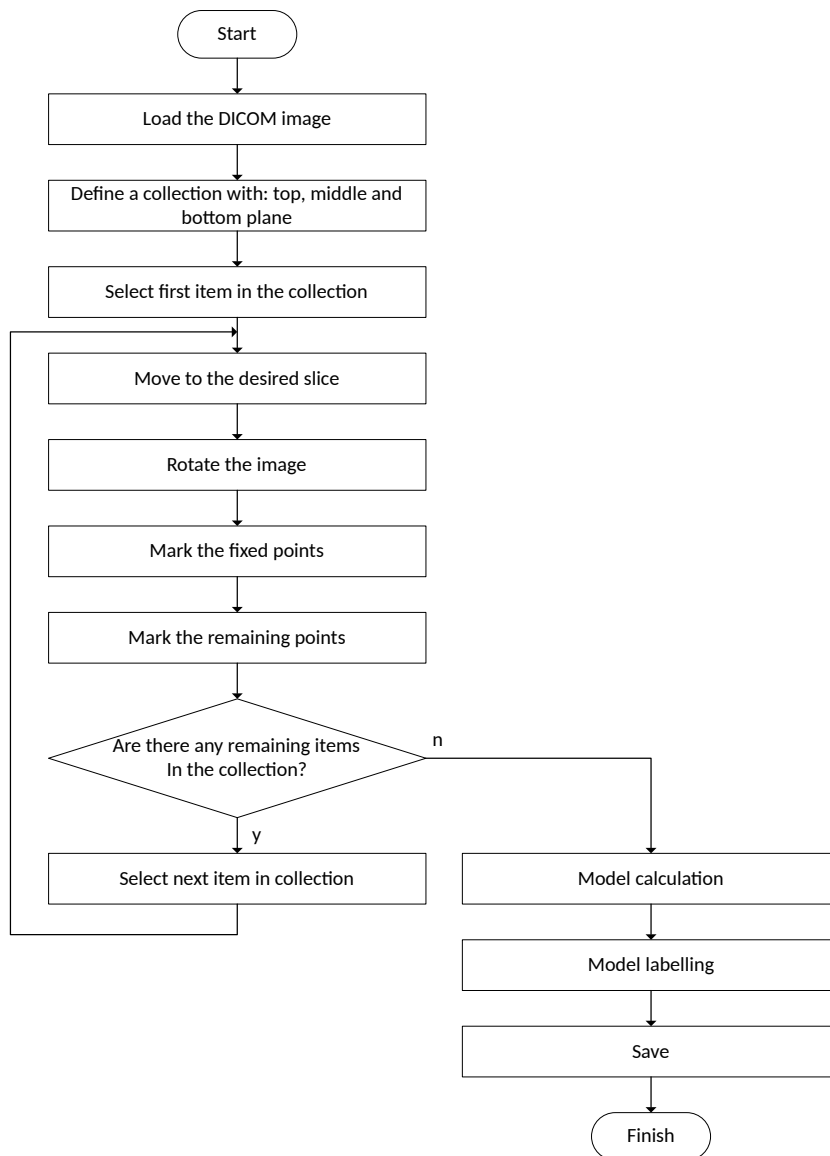


Figure 3.8: Model fitting protocol

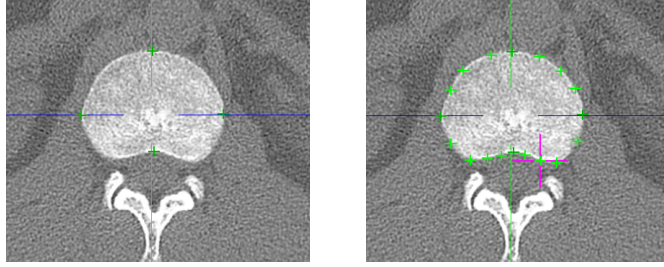


Figure 3.9: Fixed landmarks on bottom base plate (left), all landmarks on the base plate (right)

3.7 Verification process

In order to validate our model we compared the result with a ground truth. The latter was obtained together with the dataset in the form of a hand made segmentation of the vertebrae. These reference masks are available as a voxel array, therefore, to compare the final model with a reference, the model has to be voxelized. The algorithm's inputs are the desired resolution and spacing of the voxel array, which parameters are identical with the medical image parameters, and the triangular mesh representing the model. Each voxel of the 3D medical image is categorised based on whether the centre of the voxel is located inside or outside the model's closed surface. The output is generated in the previously introduced *.nrrd format.

After that the comparison was done with 3D Slicer. First the reference and exported voxel arrays are imported into the program as label maps. Then the transformation introduced in Section 3.4 is applied on the reference to rotate in the same position as the medical image. The reference mask contains the entire vertebra, but this paper focuses on the vertebral body, therefore in the next step the *processes* of the vertebra are removed from the reference with a simple cropping tool. After that various similarity metrics are calculated between the reference and the model using SlicerRT [36] extension of the 3D Slicer.

Chapter 4

Results

4.1 Developed geometric model

4.1.1 Interpolating model

After a thorough examination of the lumbar and thoracic vertebrae an elliptic cylinder shaped model was selected. This model has 3 parameters: minor axis, major axis, height. The geometrical representation was created using Catmull-Rom spline, because it is an interpolating type of spline, thus building the skeleton of the model from the axis and height can be simple. The skeleton of the model can be built from 2×4 control points, by placing one control point at both end of the axis on each base plate of the vertebra. (see Figure 4.1)



Figure 4.1: Early version of the model: cylinder model
(by Anatomy Standard[21] can be reused under the CC BY-NC 4.0[22])

This model can be further sophisticated by adding more parameters, thus making a better representation of the vertebral body. With the addition of two more parameters the side can be dented as a vertebral body's side is dented too. These two parameter would represent a scaling of the axis on the interval of $]0; 1]$. The skeleton of the model can be defined with 3×4 control points, because a middle layer had ot be added between the two base plates. (see Figure 4.2)

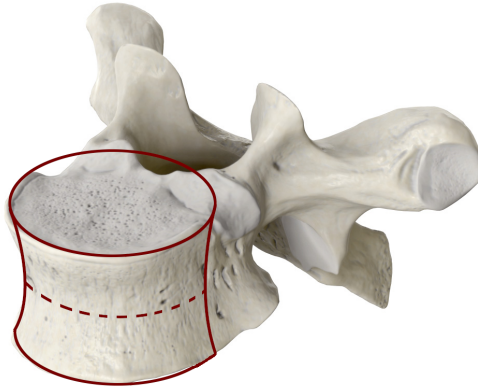


Figure 4.2: Second iteration of the model: Dented cylinder model
(by Anatomy Standard[21] can be reused under the CC BY-NC 4.0[22])

In order to represent the posterior part of the vertebral body another 2 parameters were added. These two would parametrize the posterior part of the model at the vertebral foramen (see Figure 4.3). This means the skeleton became 3×6 , as shown on Figure 4.4. In point 2 and 4 the continuity of the curve is C^0 as the derivative in these points are different on the two sides of the point.



Figure 4.3: Third iteration of the model: Posterior cut
(by Anatomy Standard[21] can be reused under the CC BY-NC 4.0[22])

In some cases the two base plate of the vertebral body are not parallel, meaning the height is not constant throughout the entire model. This tilt can be implemented by adding 3 separately controlled height to the model's anterior (0), left(1) and right (5) control points. (see Figure 4.4 and 4.5)

These implementation resulted in 9 model describing parameters. Although some of them are intuitive to set, for example the size of the axis, others are difficult to understand and determinate their correct value. Moreover after consulting with doctors and trying to fit this model the error resulting from the constraint given by the predetermined shape of the model were unacceptable. This could have been fine tuned by adding more parameters,

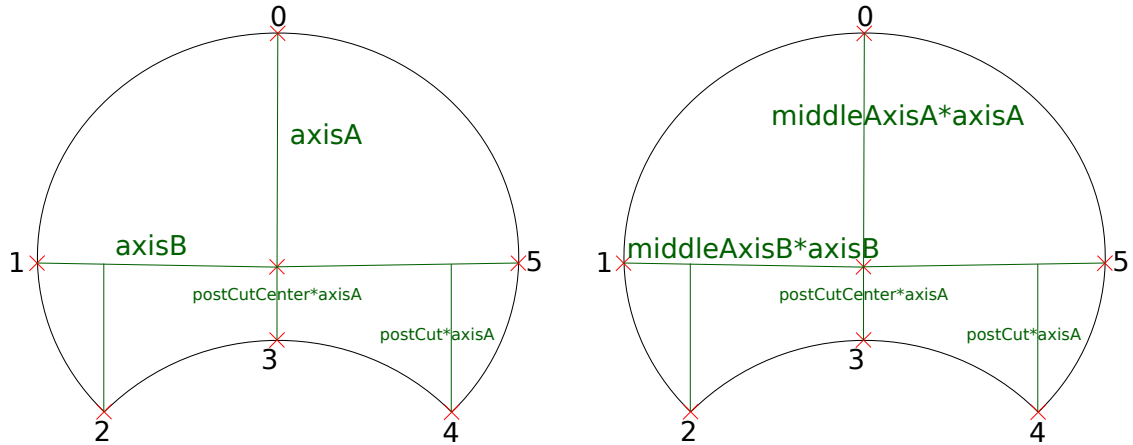


Figure 4.4: Final interpolating model:
 Base plate of the vertebra (left),
 middle plate between the two base plates (right),
 Control points numbered from 0-6, and parameters of
 the model displayed

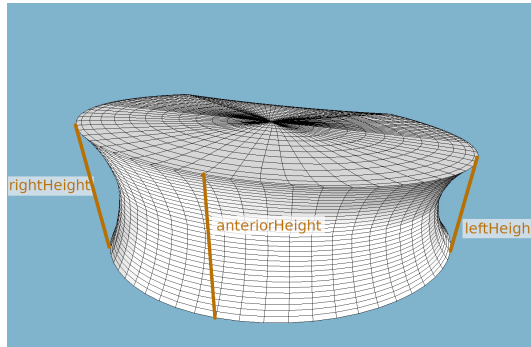


Figure 4.5: Final interpolating model:
 3 different height of the model (anterior, left, right)

but these parameters would not carry physical content, thus being hard to determinate their value. Therefore a new approach were proposed.

4.1.2 Approximating model

After a thorough discussion with doctors a fundamentally different model was designed. Instead of fixed geometrical shapes, such as the one in Section 4.1.1, the model's form would be defined entirely by curves given by markers. In predefined planes the outline of the vertebral body was marked with landmarks. Consulting with doctors we determined that 3 is the minimum necessary number of plates. The vertebral body's 2 base plates and a third one that is parallel with them. Marking the base plates are necessary to correctly represent the height of the vertebral body, while the middle plane is essential for modelling the dent of the vertebral body. Figure 4.6 shows these planes.

Doctors proposed to mark 18 points in each planes. The final implementation allows to use less than 18 points, however, the 3 planes are enforced. Figure 4.8 shows the recommended position of these points. After placing these landmarks, they have to be ordered. There is no constraint toward the user to mark them in clockwise or any predefined series, but

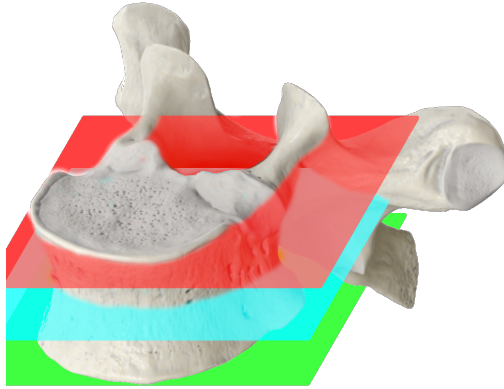


Figure 4.6: 3 planes on the vertebra,
 Red: base plate of the vertebra,
 Green: bottom base plate of the vertebra,
 Blue: middle plane between the two base plates
*(by Anatomy Standard[21] can be reused under the CC
 BY-NC 4.0[22])*

the curve fitting algorithm requires the points to be in order. Thus we have defined and implemented an ordering method achieving the ordered set of points in 6 steps (see Figure 4.7):

1. Calculating the centroid of the marked points.
2. Applying an offset to shift the origo of the coordinate system into the centroid.
3. Converting from Cartesian coordinate system into cylinder coordinate system.
4. Sort the coordinates by the φ angel.
5. Convert back to Cartesian coordinate system.
6. Apply the invert of step 2.

This algorithm has a limitation when the z axis of the coordinate system lines up width the plane defined by the markers, but in the vertebral column the orientation of the vertebrae rules this scenario is absolutely unlikely. However, adding a step where the plane's normal vector is rotated to line up with the z axis would solve this issue.

As next step a curve fitting algorithm defines a closed B-spline curve with a given degree of freedom [37]. The algorithm defines a least square error cost function and in an iterative process the residual calculated based on this weighted cost function is reduced. In our analysis we used 12th degree splines, as it resulted in an accurate approximation of the landmarks, while eliminating any wiggles caused by the uneven placement of the landmarks. The fitting algorithm can give weights to the landmark points and those weighted markers will be approximated with negligible error. In the 18 point design the two axis of the elliptic shaped base plate are given higher value (red markers on Figure 4.8), thus approximating them with significantly lower error.

After testing this method with several data sets an optimisation step was added, because the fitting algorithm yielded different results based on which marker was the initial landmark. An optimisation method is defined which calculates each marker's distance from

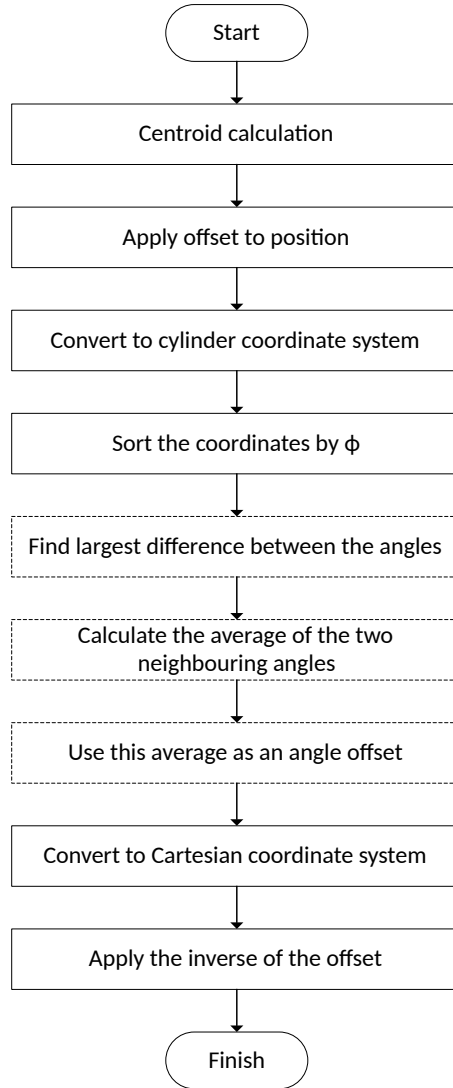


Figure 4.7: The method of ordering of the marker points

the curve used the well known Newton method [38]. Then for each landmarks its minimal distance from the spline is calculated and the maximum of these distances are stored as a score of the given configuration. After this step the array of landmarks rotated, thus making the first element the last, and the originally second element become the first. In this new configuration a score is calculated the same way as before. This process is repeated until the landmark array is fully rotated, than the configuration with the lowest score is selected.

In order to generate a mesh for visualization of the geometrical model, the 3 spline's has to be align. This can be achieved using the landmarks as base points in the alignment process. The belonging landmarks on the 3 planes are located below each other. Since the sorting method, introduced above, will start at 0° there could be a scenario when this algorithm fails. For example on the top plane the anterior marker is placed at 1° , while on the bottom plane at 359° , thus making the first point on the top, and the last one on the bottom. This is mitigated by adding an extra step to the algorithm. After sorting the top plane the largest difference between 2 neighbouring points φ coordinate is looked up, and the average of these 2 points φ coordinates taken as an offset. This offset than applied on each 3 planes to shift the points and align the belonging ones together.

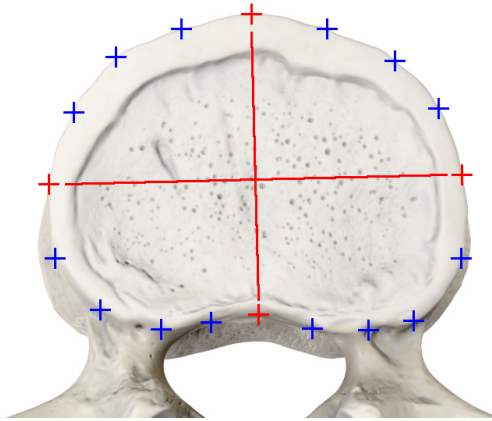


Figure 4.8: Landmark position on the vertebral body,
 Red: fixed points, blue: approximated point
*(by Anatomy Standard[21] can be reused under the CC
 BY-NC 4.0[22])*

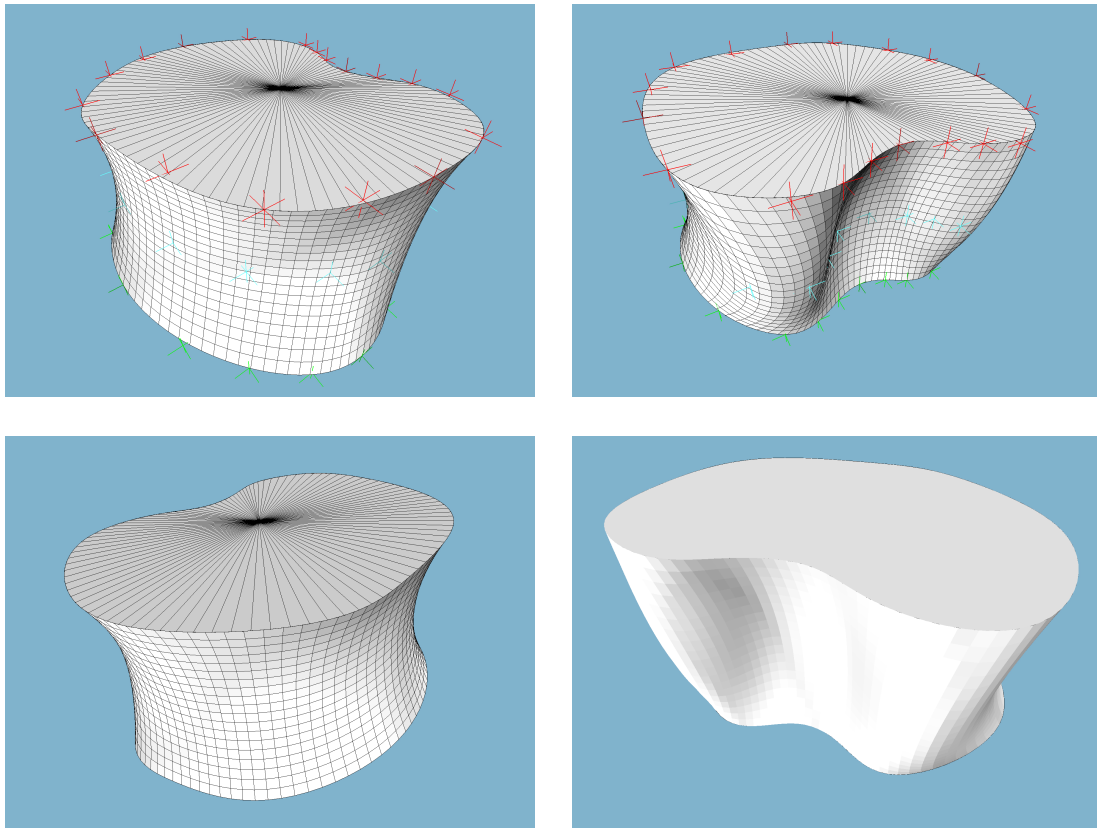


Figure 4.9: Approximating model (L1 vertebra of Subject01)

This process requires that each plane to have its landmarks selected at the same position within the vertebra. Then using these associated landmarks the closest point on the curve can be sought for each landmark with the aforementioned distance finding algorithm. This algorithm's output is a t scalar value giving the position on the curve. Because in this application the splines are closed the t value can be interpreted as an angle too. Calculating the average difference between these angles will provide an offset between the two splines. Selecting one spline out of the 3 as a reference and computing the other

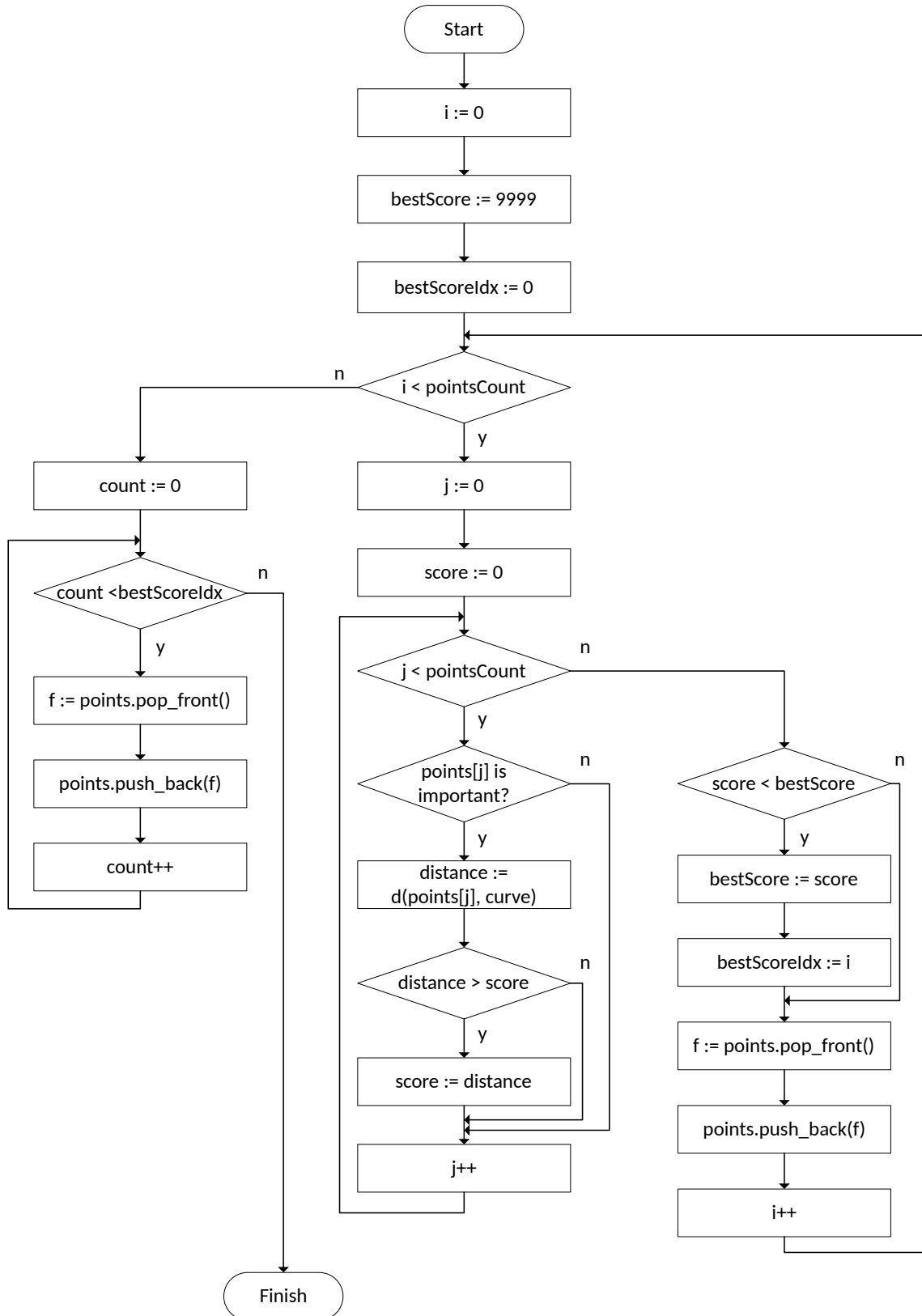


Figure 4.10: Optimisation algorithm to minimize the error of fitting

two's offset from it will produce a coherent 3 splines system, that can be used for mesh generation for visualization.

Following the examination of the vertebrae anatomy and discussing the topic with doctors we came to the conclusion that a quadratic function would be accurate enough to describe the shape of the model's side. Therefore side of the model is defined by a quadratic function between the 3 splines mentioned earlier.

The resulting model is robust and versatile, that is capable to represent all individually standing vertebra in the spinal column. Figure 4.9 shows the final model in use.

4.2 Model verification results

Following a discussion with doctors revealed that 6 out of the 10 patients in the database has a degenerative lumbar spine. Our goal in this paper was to analyse healthy vertebrae, therefore the remaining 4 was selected. The modelling of these 20 vertebrae was done using the model introduced in Section 4.1.2. After that a comparison was done as described in Section 3.7 and visualized on Figure 4.11. Dice coefficient and Hausdorff distance metrics (introduced in Section 3.5) were used in the evaluation.

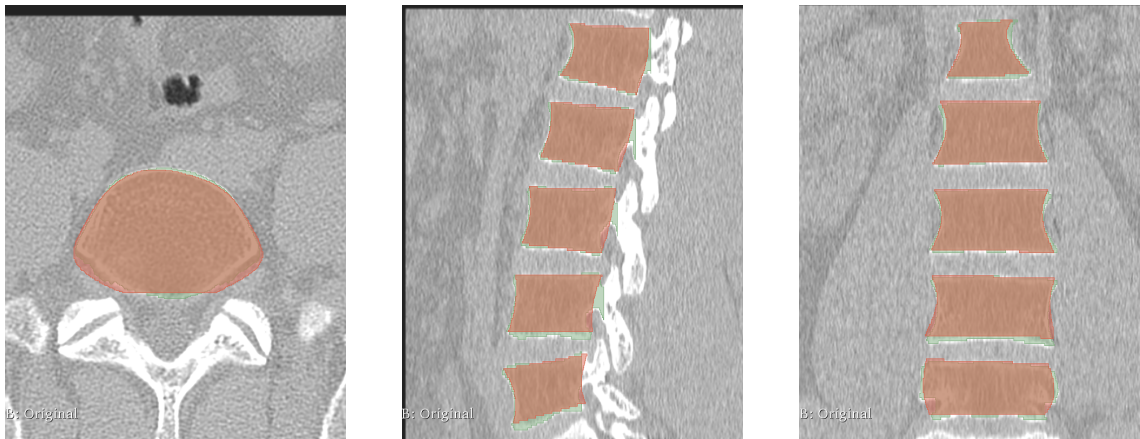


Figure 4.11: Comparison in axial (left), sagittal (middle) and coronal (right) view.
(Green: reference, red: model)

The results with Hausdorff metric are summarized in Table 4.1. in Figure 4.12 the Hausdorff maximum values are shown, where outliers with greater than one standard deviation away from mean of the dataset are marked with red circle.

The results with Dice coefficient are summarised in Table 4.2.

Other key criteria towards the model is an efficient and fast model fitting process. Our measurements indicate, that roughly 1 hour is required to model the lumbar section of a spinal column including 5 vertebrae, thus the average time to define the patient specific geometric model of a vertebra is around 12 minutes.

4.3 Validation of the model for solving medical problems

This paper's goal is not to provide a detailed medical analysis, rather to demonstrate the possible use cases of the suggested geometrical model. Table 4.3 shows the volume of the individual vertebrae which is a parameter that can not be measured with a typical medical image visualization system obtained from the model. Table 4.4 presents the volume of the

Subject	Vertebra	Max [mm]	Avg [mm]	95% [mm]
Subject01	L1	4.95	0.53	1.24
Subject01	L2	5.59	0.71	2.14
Subject01	L3	6.48	0.64	1.92
Subject01	L4	9.79	1.13	2.86
Subject01	L5	4.29	0.99	2.96
Subject06	L1	6.12	2.01	3.53
Subject06	L2	6.11	1.96	3.83
Subject06	L3	4.59	1.66	3.26
Subject06	L4	5.20	1.51	3.63
Subject06	L5	6.95	1.35	3.22
Subject08	L1	4.01	0.93	2.72
Subject08	L2	4.01	0.94	2.62
Subject08	L3	4.98	1.14	3.10
Subject08	L4	4.08	0.91	2.03
Subject08	L5	6.43	1.04	2.63
Subject10	L1	5.54	0.94	2.73
Subject10	L2	6.30	1.09	2.53
Subject10	L3	4.26	1.07	2.23
Subject10	L4	4.81	1.21	2.85
Subject10	L5	17.10	1.60	4.00
Average		6.08	1.17	2.80
Standard deviation		2.93	0.40	0.69

Table 4.1: Model comparison with reference using Hausdorff metric

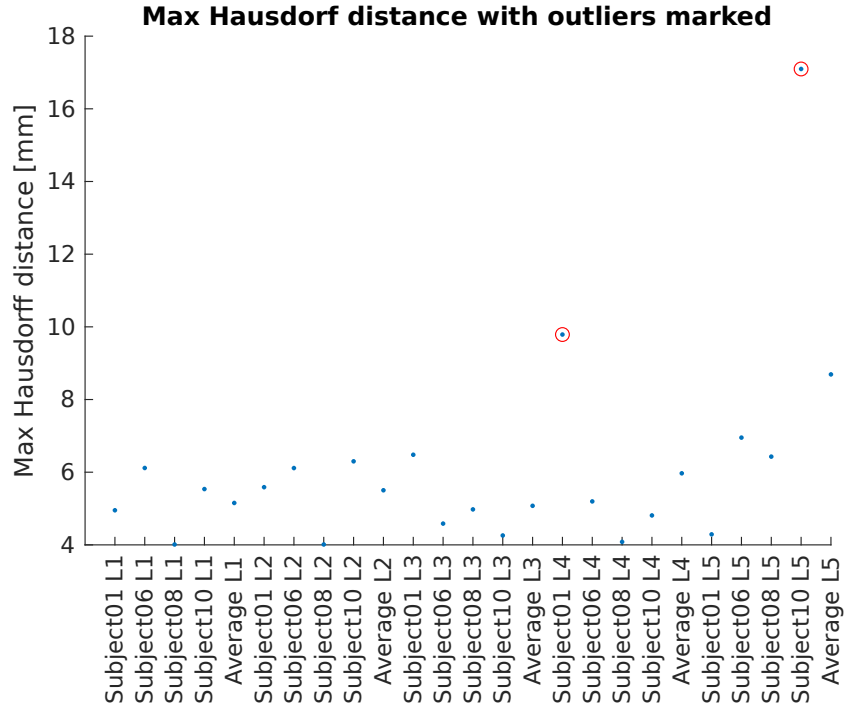


Figure 4.12: Hausdorff maximum with outliers marked with red circle

Subject	Vertebra	Dice coeff	True pos+neg [%]	False pos [%]	False neg [%]
Subject01	L1	0.94	94.44	1.53	4.03
Subject01	L2	0.93	93.07	3.27	3.65
Subject01	L3	0.93	92.83	2.32	4.86
Subject01	L4	0.90	89.61	2.08	8.30
Subject01	L5	0.91	92.34	1.52	6.14
Subject06	L1	0.82	85.32	6.27	8.40
Subject06	L2	0.84	85.95	6.53	7.52
Subject06	L3	0.85	86.42	6.89	6.69
Subject06	L4	0.86	87.93	4.08	7.99
Subject06	L5	0.84	90.01	4.51	5.48
Subject08	L1	0.92	92.93	1.68	5.39
Subject08	L2	0.92	92.72	2.07	5.21
Subject08	L3	0.90	90.06	2.08	7.86
Subject08	L4	0.92	91.57	2.19	6.25
Subject08	L5	0.89	91.40	1.77	6.83
Subject10	L1	0.90	93.05	4.08	2.87
Subject10	L2	0.89	91.50	3.00	5.50
Subject10	L3	0.89	90.14	3.36	6.50
Subject10	L4	0.87	88.29	2.29	9.41
Subject10	L5	0.82	94.33	0.85	4.82
Average		0.89			
Standard deviation		0.04			

Table 4.2: Model comparison with reference using Dice metric

Subject	L1 [cm^3]	L2 [cm^3]	L3 [cm^3]	L4 [cm^3]	L5 [cm^3]
Subject01	37.13	40.52	43.03	44.27	38.79
Subject06	27.25	29.11	31.20	27.80	27.99
Subject08	30.60	33.34	35.32	38.56	35.25
Subject10	29.78	31.95	33.95	30.69	27.08
Average	31.19	33.73	35.88	35.33	32.28
Standard deviation	4.21	4.86	5.07	7.50	5.68

Table 4.3: Volume of vertebrae calculated from the model

Subject	L1 [cm^3]	L2 [cm^3]	L3 [cm^3]	L4 [cm^3]	L5 [cm^3]
Subject01	39.12	40.85	45.12	49.87	43.26
Subject06	28.74	29.79	31.06	30.47	28.89
Subject08	33.38	35.84	39.57	41.60	39.89
Subject10	28.77	34.16	36.40	35.89	34.65
Average	32.50	35.16	38.04	39.46	36.67
Standard deviation	4.92	4.57	5.88	8.30	6.28

Table 4.4: Volume of vertebrae calculated from the reference

reference used in the validation process. In Table 4.5 the inaccuracy of the generated patient specific models can be seen described by the volume difference between the model volume and the volume of the reference. However the amount of data is not adequate to

Subject	L1 [cm^3]	L2 [cm^3]	L3 [cm^3]	L4 [cm^3]	L5 [cm^3]
Subject01	1.99 (5.1%)	0.33 (0.8%)	2.09 (4.6%)	5.60 (11.2%)	4.47 (10.3%)
Subject06	1.49 (5.2%)	0.67 (2.3%)	0.14 (0.4%)	2.67 (8.8%)	0.90 (3.1%)
Subject08	2.78 (8.3%)	2.50 (7.0%)	4.24 (10.7%)	3.04 (7.3%)	4.64 (11.6 %)
Subject10	1.01 (3.5%)	2.21 (6.5%)	2.44 (6.7%)	5.20 (14.5%)	7.58 (21.9%)
Average	1.82 (5.6%)	1.43 (4.1%)	2.23 (5.9%)	4.13 (10.5%)	4.40 (12.0%)
Std. dev.	0.76	1.08	1.68	1.48	2.73

Table 4.5: Difference in the volume of vertebrae calculated from the model compared with the reference

make detailed statistical analysis, the data at hand shows great variability between the size of the vertebrae as mentioned in Section 2.1.3.

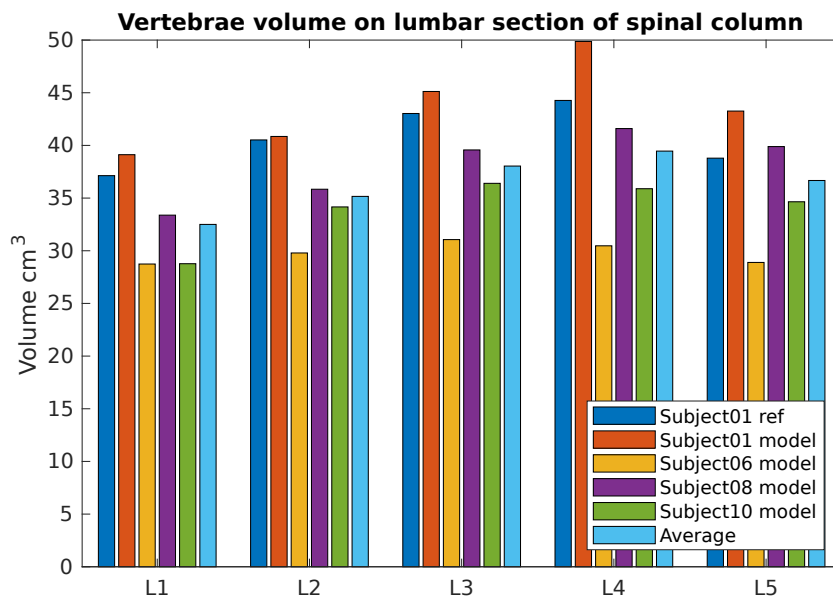


Figure 4.13: Volume of the vertebrae (measured on the model)

4.4 Framework

The implementation of a modelling framework was necessary for managing and efficiently execute and test the model fitting. For this purpose an environment originally built for aortic valve modelling [39] was used. Although the task is different from medical perspective, there are lot of similarities in the engineering requirements. Both of them are a modelling task, where a model has to be co-registered with the medical image.

The original framework were design as a cross platform compatible system. This feature were retained, thus the framework can run on Linux or Microsoft Windows operation system.

There are 2 main and 1 auxiliary workflows in the software, to which belong 3 different views. Figure 4.14 shows the main structure of the software's layout, with a 3D view in the centre and a workflow specific window on the left side of the screen.

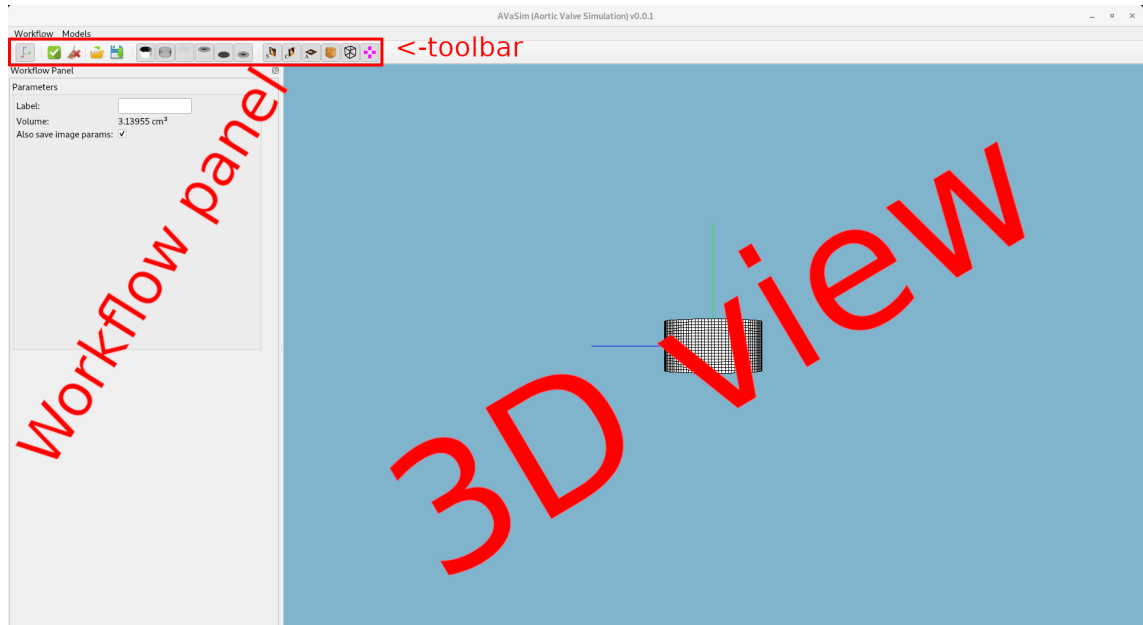


Figure 4.14: Framework layout

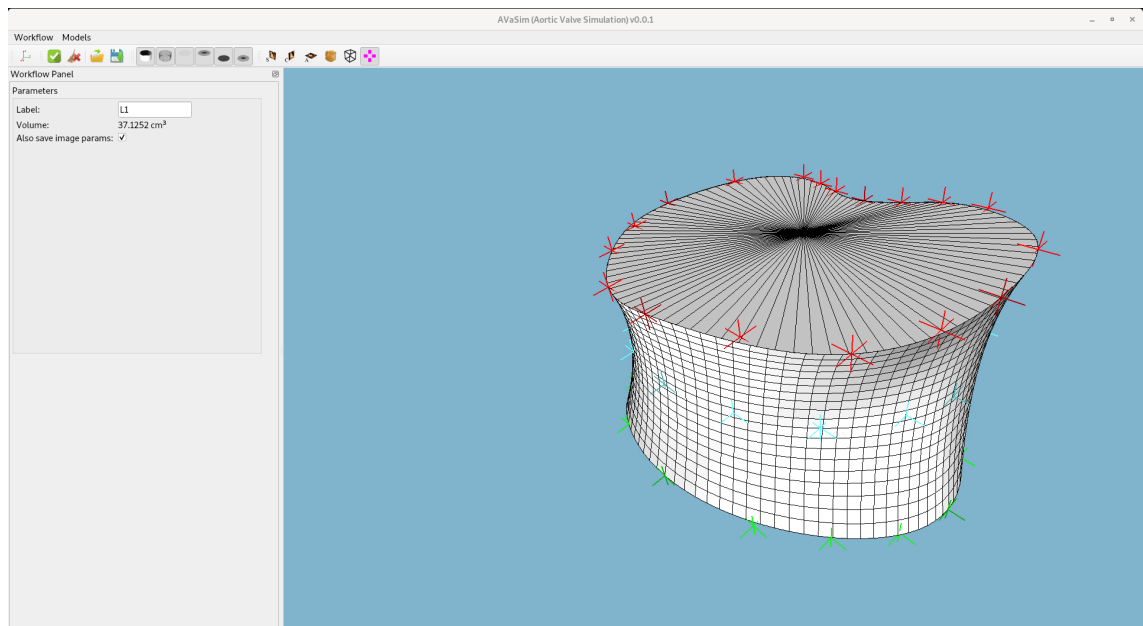


Figure 4.15: Modelling layout of the modelling framework

In medical image workflow the user can load DICOM images, which is one of the most widespread medical image data format. This workflow has, in addition to the 3D view, two 2D views too, showing the medical image in different slice directions. These 2D views allows the user to move between the slices, rotate the image and place markers for measurement or model fitting purposes. The workflow window has 4 menus, as shown on Figure 4.17:

1. Volume: containing the most important parameters of the medical image, such as spacing and resolution.

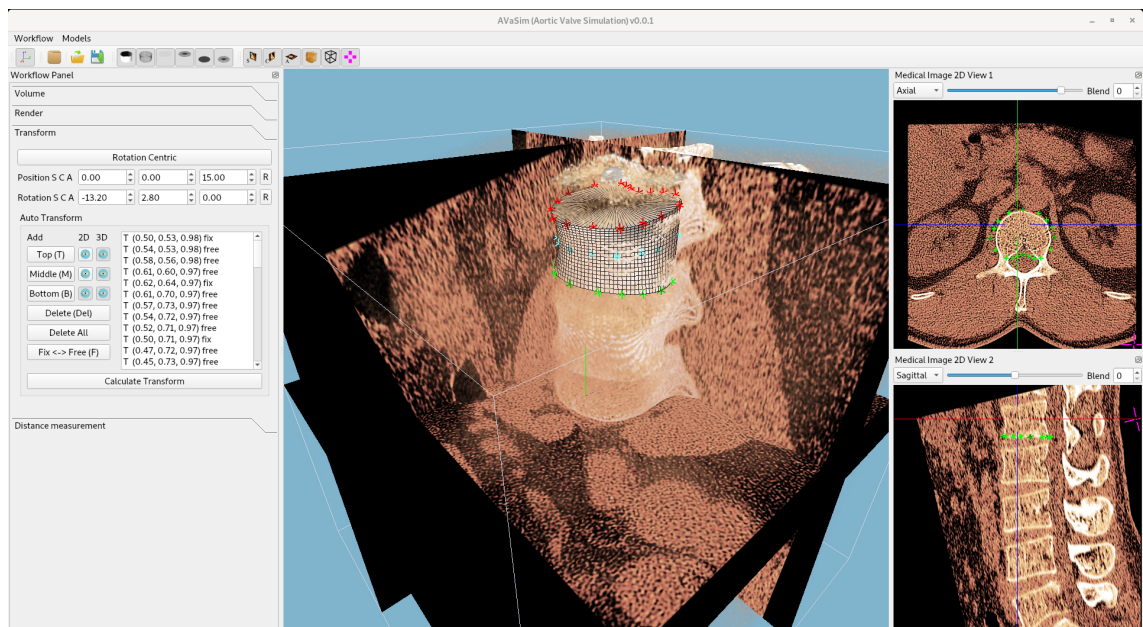
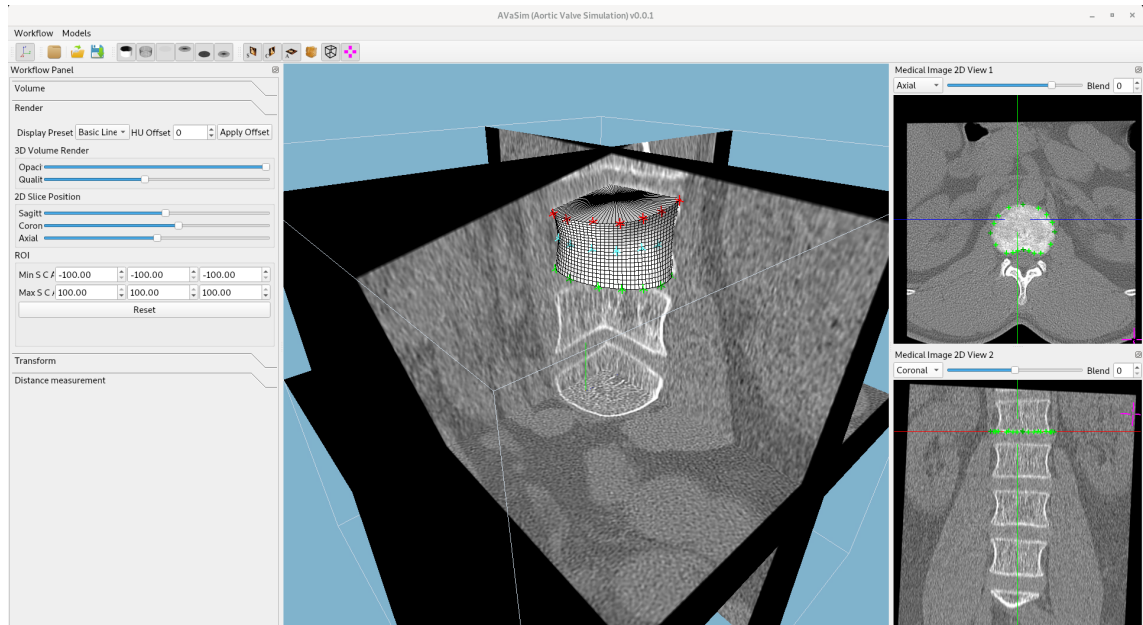


Figure 4.16: Medical image layouts of the modelling framework showing examples for visualizing the marked landmarks

2. Render: displaying the options related to the image visualization, e.g. preset control, and ROI (Region of Interest) selection.
3. Transform: the collection of options to control the position and offset of the image, and provides control for the user placeable landmarks for the model fitting process introduced in Section 4.1.2.
4. Distance measurement: the user interface for distance measurement between two user placeable landmarks on the image.

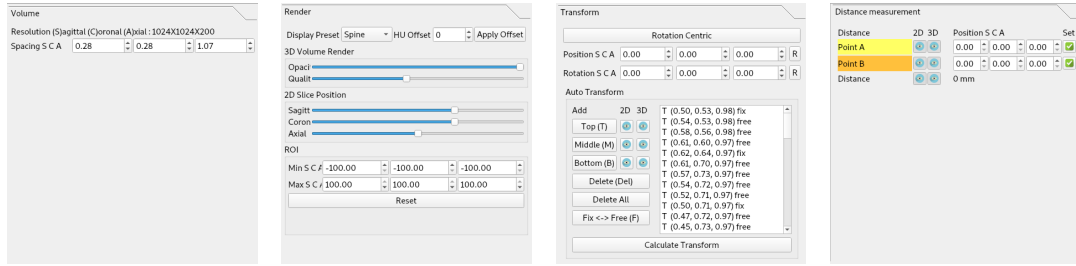


Figure 4.17: Medical image panels in the modelling framework used to define the patient specific parameters of the geometric model

In modelling layout the model related parameters and controls are accessible (see Figure 4.15). In case of a vertebra model this window has an input label field to manually enter which vertebra is being modelled in the spinal column. In case of aortic valve modelling the model defining parameters (size, angle) can be set here.

The third workflow hosts the controls for model exportation, either as a triangular mesh in *.obj file, or a voxel array in *.nrrd file.

The original framework were enhanced to better suit the needs of this research. Support for multiple models were added to remain useable for aortic valve modelling and to simplify the comparison between different vertebral body models in the development stage. As recommended by medical professionals a feature to easily and intuitively rotate the medical image on the 2D view were implemented. This allows the rotation of the 2D view precisely into the plane of the vertebral body's base plate, which is not necessary parallel with the axial slice of the image. That greatly improves the process of landmark placement on anatomical points. On top of these, numerous features were added based on the doctors recommendation. The development process required closed collaboration with them, to be able to as quickly as possible implement and integrate these new functions. Thanks to this agile development process an ergonomic and scaleable platform were created for vertebra modelling.

Chapter 5

Discussion

Our goal in this paper was to develop an accurate geometric model of the vertebra body that can be easily fitted and simple to use. An iterative and agile development process was utilized where we frequently discussed the achieved results with medical experts. The accuracy of the model can be measured with high degree of precision when a reference mask is available. The achieved accuracy of the model is presented in Table 4.1 and 4.2. In case of Hausdorff distance the best achievable result is limited by the voxel spacing. As mentioned in Section 3.7 the voxels are categorized into two classes based on whether the centre of the voxel is inside the close shape of the model or outside of it. This means the theoretical limit is set by the spacing between the voxels of the 3D image. In our research this data is summarized in Table 3.1. The average voxel size was $0.412 \times 0.412 \times 1.043 \text{ mm}$ (0.177 mm^3) in our experiments.

One major limiting factor in the validation process were originated from the fact that the reference mask contained the entire vertebra, while the modelling covered only the vertebral body. To overcome this issue the *processes* were cropped from the reference mask, but since it is hard to unambiguously differentiate the vertebral body from the *pedicle of vertebral arch* (see Figure 2.3), an error were introduced to the validation process at this stage, causing lower scores than possible. Another potential error were introduced into the validation process since these excess parts of the vertebra were cut of with a vertical plane. This does not cause significant distortion when examining the upper section of the lumbar spine, where the vertebrae are lined up with the horizontal plane, however, at the lower section of the lumbar spine (typically at L4 and L5 vertebrae) this does not remain true as shown on Figure 5.1. This inaccuracy could slightly reduce the measured precision of the model. This was the most probable cause of the two outlier data points presented on Figure 4.12. This assumption is further supported by the fact there is an observable tendency (as also presented on Figure 4.12) of the L3 vertebra being the closest to a horizontal position.

On top of this there are lots of limiting factors which slightly degrades the model's precision. Small details on the surface are lost due to the fact that the landmarks are placed only in 3 planes. The model assumes that the base plate is completely flat, however, in reality it has some imperfections. Worth taking into consideration the B-splines as limiting factors too, as the shape of the vertebra not necessary follows the B-spline. The quadratic function defining the side of the model falls into the same category, since the vertebral body's side can only be approximated with a second degree polynomial. These limitations are inherently coming from the model, but the final model's accuracy depends on the user's precision too. Error could be introduced if the rotation of the planes are not

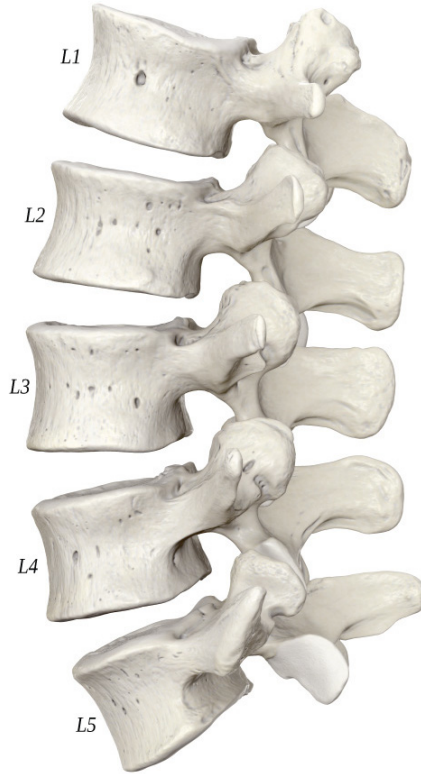


Figure 5.1: Lumbar section of the spinal column
(by Anatomy Standard[21] can be reused under the CC BY-NC 4.0[22])

perfectly lined up with the base plate of the vertebral body, the markers are not placed consistently enough or perfectly at the edge of the vertebra. Despite the difficulties described above the Dice coefficient reached an average of $88.7 \pm 3.8\%$ and the Hausdorff metric achieved $2.8 \pm 0.69 \text{ mm}$ on the 95% of the model which is considered to be very accurate compared to results published in papers dealing with similar problems. The Dice similarity coefficient comparison between our results and results published in the literature are as follows:

- $88.7 \pm 3.8\%$ result of the current research,
- $82.99 \pm 5.03\%$ J. Egger et al. [2],
- $90.97 \pm 2.2\%$ J. Egger et al. [3],
- $94.94 \pm 1.69\%$ P. H. Lim et al. [16],
- $91.0 \pm 7.0\%$ C. Chengwen et al. [17],
- $94.3 \pm 3.2\%$ M. Vania et al. [18].

Figure 5.2 shows a 3D visualization of the reference mask (presented with green) and the model created during this study (presented with red) in an overlay. The error caused by the cropping of the reference mask (as described in the previous section) is clearly visible on the first and the last image. The error caused by the simplification made on the surface of the vertebral body's base plate is also observable. The healthy vertebral body's base plate has a slightly risen edge, which was not taken into consideration in this model. On

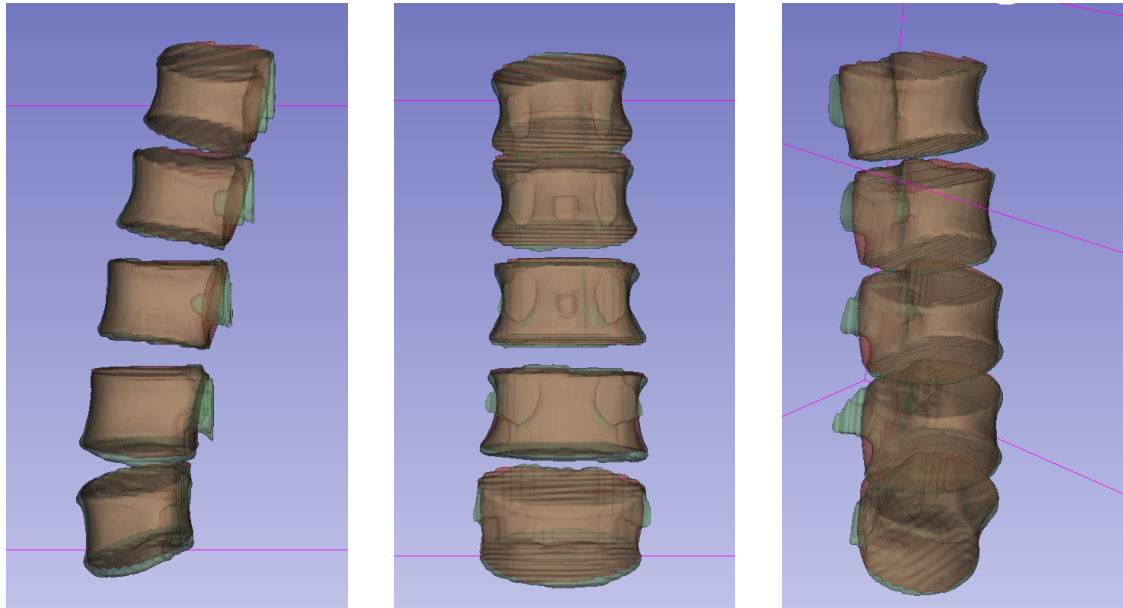


Figure 5.2: 3D comparison of the model and reference in 3D Slicer
(Subject01)
Green: reference, red: model

top of these there is a visible mismatch on the side of the model too, introduced by the quadratic function that defines this part of the geometrical model.

Key expectation toward the model and framework was to create an easily and efficiently useable system. Ease of use can not be quantitatively measured, it depends on the personal opinion of the medical professional. The two key steps that needs to be evaluated are the intuitiveness of the image rotation and landmark placement. Based on doctors feedback the ergonomics of the software were greatly improved with the addition of small features. The time necessary to fit the model can be measured, nearly 1 hour necessary to analyse the lumbar section of the spinal column. That means roughly 12 minutes for each vertebra.

The final model is well suited for making clinical analysis and researches. Not only the individual vertebra can be analysed with this model, but the entire spinal column too, including the intervertebral space. Therefore measurement introduced on Figure 1.1 could be easily and automatically evaluated. Moreover, complex parameters, such as area and volume of the vertebra can be calculated too.

Chapter 6

Conclusions

In this paper a novel geometrical model of the human vertebral body, that can be co-registered with a 3D medical image was suggested. Along with this, an optimal surface fitting algorithm enabling an easy and accurate model definition and parameter optimisation algorithm were developed and implemented. The geometrical model and the associated methods were validated on a standard database with 20 vertebrae. The usability of the proposed model in clinical research were demonstrated in a small size clinical study. The presented results could be used in the analysis of alternative treatment methods of the vertebral body compression fracture. The B-spline representation of the model could be fitted with the marking of special anatomical points. As a technical result a complete modelling framework were created. A geometrical model and the application of a clinical protocol were defined that can be used in future result projects as well. The validation of the process and the vertebral model has been done, resulting in a highly accurate geometrical model. Therefore, the final model could be used in clinical studies of the vertebrae and spinal column. The proposed geometrical model of the vertebral body could be used as uniform representation of all kind of vertebra, such a model has not been published in previous studies.

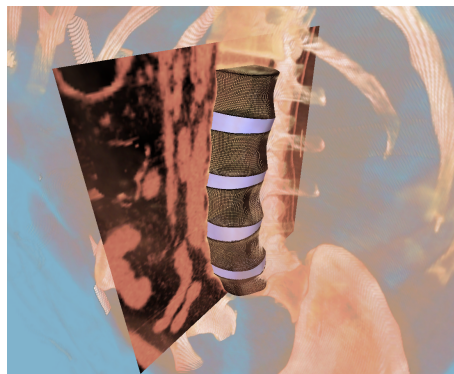


Figure 6.1: Lumbar spine model showing the defined patient specific geometric model of the corresponding vertebrae. The co-registration with the original CT image can be also seen.

In the first part of this paper a brief overview of the current state of the human vertebrae modelling were presented, and these study's limitation were discussed. Following that a summary over the anatomy of the spinal column is given. The compression fracture of the vertebral body and a treatment option also presented, along a problem that requires

the modelling of the vertebral body. In the 3rd chapter the necessary methods for the modelling displayed. This part of the paper presented the data used for the validation process. In the next chapter the results are summed up starting with the completed model, outlining the verification process and the framework used for the model fitting. Finally, the achieved results are discussed.

6.1 Further work

Our plan for the future is to verify the model on cervical and thoracic part of the spinal column, thus proving the model suitable for modelling the entire human spinal column. Along this the evaluation of usability on injured and fractured vertebra should be done, in order to make applicable for all type of researches on the vertebral column. The model can be extended to the entire vertebra instead of only modelling the vertebral body, therefore becoming possible to analysis conditions related to the *spinal canal* or the *processes* of the vertebra. The modelling framework can be improved too in order to further simplify its usage and implement automated steps, thereby accelerate the whole workflow.

Studying the compression fracture of the vertebra (introduced in Section 2.1.2) using this novel geometrical model to determine the original height and volume of a compressed vertebra based on the neighbouring uninjured ones. That way giving a recommendation to improve the medical procedure nowadays used for its treatment.

Acknowledgements

I would like to thank my advisors, Prof. Balázs István Benyó, Dr. Ákos Szlávecz, Dr. Árpád Viola for their work and help that made this paper possible.

I would also like express my gratitude to Dr. Tamás Umenhoffer for helping me setup the framework, assisting and giving advices for it's usage.

I am grateful for Prof. Tamás László Várady and Dr. Péter Salvi for their help in the design of the model and for so kindly supporting me in the creation of the model fitting algorithm.

Bibliography

- [1] Mohammed Benjelloun, Mahmoudi Saïd, and Fabian Lecron. A framework of vertebra segmentation using the active shape model-based approach. *International journal of biomedical imaging*, 2011:621905, 07 2011.
- [2] J. Egger, C. Nimsky, and X. Chen. Vertebral body segmentation with Grow-Cut: Initial experience, workflow and practical application. *SAGE Open Med*, 5:2050312117740984, 2017.
- [3] Jan Egger, Tina Kapur, Thomas Dukatz, Malgorzata Kolodziej, Dženan Zukić, Bernd Freisleben, and Christopher Nimsky. Square-cut: A segmentation algorithm on the basis of a rectangle shape. *PloS one*, 7:e31064, 02 2012.
- [4] V Divya and Anburajan Mariamichael. Finite element analysis of human lumbar spine. *ICECT 2011 - 2011 3rd International Conference on Electronics Computer Technology*, 3, 04 2011.
- [5] Michael Fagan, S Julian, and Amr Mohsen. Finite element analysis in spine research. *Proceedings of the Institution of Mechanical Engineers. Part H, Journal of engineering in medicine*, 216:281–98, 02 2002.
- [6] Miomir Lj. Jovanović Janko D. Jovanović. Biomechanical model of vertebra based on bone remodeling. *Medicine and Biology*, 11:35–39, 2004.
- [7] C. Lorenz and N. Krahnstover. 3d statistical shape models for medical image segmentation. pages 414–423, 1999.
- [8] Bulat Ibragimov, Bostjan Likar, Franjo Pernus, and Tomaž Vrtovec. Shape representation for efficient landmark-based segmentation in 3-d. *Medical Imaging, IEEE Transactions on*, 33:861–874, 04 2014.
- [9] S. Huang, Y. Chu, S. Lai, and C. L. Novak. Learning-based vertebra detection and iterative normalized-cut segmentation for spinal mri. *IEEE Transactions on Medical Imaging*, 28(10):1595–1605, 2009.
- [10] Yiebin Kim and Dongsung Kim. A fully automatic vertebra segmentation method using 3d deformable fences. *Computerized medical imaging and graphics : the official journal of the Computerized Medical Imaging Society*, 33(5):343–352, July 2009.
- [11] Darko Štern, Boštjan Likar, Franjo Pernuš, and Tomaž Vrtovec. Parametric modelling and segmentation of vertebral bodies in 3d ct and mr spine images. *Physics in medicine and biology*, 56:7505–22, 11 2011.
- [12] Darko Štern, Bostjan Likar, Franjo Pernus, and Tomaž Vrtovec. Automated detection of spinal centrelines, vertebral bodies and intervertebral discs in ct and mr images of lumbar spine. *Physics in medicine and biology*, 55:247–64, 01 2010.

- [13] Robert Korez, Bulat Ibragimov, Bostjan Likar, Franjo Pernus, and Tomaž Vrtovec. A framework for automated spine and vertebrae interpolation-based detection and model-based segmentation. *IEEE transactions on medical imaging*, 34, 01 2015.
- [14] A. Rasoulia, R. Rohling, and P. Abolmaesumi. Lumbar spine segmentation using a statistical multi-vertebrae anatomical shape+pose model. *IEEE Transactions on Medical Imaging*, 32(10):1890–1900, 2013.
- [15] Jun Ma, Le Lu, Yiqiang Zhan, Xiang Zhou, Marcos Salganicoff, and Arun Krishnan. Hierarchical segmentation and identification of thoracic vertebra using learning-based edge detection and coarse- to-fine deformable model. *Medical image computing and computer-assisted intervention : MICCAI ... International Conference on Medical Image Computing and Computer-Assisted Intervention*, 13:19–27, 01 2010.
- [16] P. H. Lim, U. Bagci, and L. Bai. Introducing willmore flow into level set segmentation of spinal vertebrae. *IEEE Transactions on Biomedical Engineering*, 60(1):115–122, 2013.
- [17] Chu Chengwen, Daniel Belavy, Gabi Ambrecht, Paul Bansmann, Dieter Felsenberg, and Guoyan Zheng. Fully automatic localization and segmentation of 3d vertebral bodies from ct/mr images via a learning-based method. *PLOS ONE*, 10:e0143327, 11 2015.
- [18] Malinda Vania, Dawit Mureja, and Deukhee Lee. Automatic spine segmentation from ct images using convolutional neural network via redundant generation of class labels. *Journal of Computational Design and Engineering*, 6(2):224 – 232, 2019.
- [19] Algirdas Maknickas, Vidmantas Alekna, Oleg Ardatov, Olga Chabarova, Darius Zabulionis, Marija Tamulaitiene, and Rimantas Kačianauskas. Fem-based compression fracture risk assessment in osteoporotic lumbar vertebra l1. *Applied Sciences*, 9:3013, 07 2019.
- [20] Fabio Galbusera, Gloria Casaroli, and Tito Bassani. Artificial intelligence and machine learning in spine research. *JOR SPINE*, 2:e1044, 02 2019.
- [21] Website: Anatomy standrard. <https://www.anatomystandard.com/>. Accessed: 2020-10-28.
- [22] Cc by-nc 4.0 licence. <https://creativecommons.org/licenses/by-nc/4.0/>. Accessed: 2020-10-28.
- [23] Sergei Pravdin. A mathematical spline-based model of cardiac left ventricle anatomy and morphology. *Sciprints*, 10 2016.
- [24] S. Barone, A. Paoli, and A. V. Razionale. CT segmentation of dental shapes by anatomy-driven reformation imaging and B-spline modelling. *Int J Numer Method Biomed Eng*, 32(6), 06 2016.
- [25] S. Sandor and R. Leahy. Surface-based labeling of cortical anatomy using a deformable atlas. *IEEE Transactions on Medical Imaging*, 16(1):41–54, 1997.
- [26] L. Zhi, J. Yan, T. Zhou, and Q. Tang. Tongue shape detection based on b-spline. pages 3829–3832, 2006.
- [27] P. Brigger, J. Hoeg, and M. Unser. B-spline snakes: a flexible tool for parametric contour detection. *IEEE Transactions on Image Processing*, 9(9):1484–1496, 2000.

- [28] Aaron Babb and Walter Carlson. Vertebral compression fractures: Treatment and evaluation. *South Dakota medicine : the journal of the South Dakota State Medical Association*, 59:343–5, 347, 09 2006.
- [29] James Langdon, Adam Way, Samuel Heaton, Jason Bernard, and Sean Molloy. Vertebral compression fractures - new clinical signs to aid diagnosis. *Annals of the Royal College of Surgeons of England*, 92:163–6, 12 2009.
- [30] Cc by 3.0 licence. <https://creativecommons.org/licenses/by/3.0/>. Accessed: 2020-10-28.
- [31] L. J. Melton, S. H. Kan, M. A. Frye, H. W. Wahner, W. M. O’Fallon, and B. L. Riggs. Epidemiology of vertebral fractures in women. *Am. J. Epidemiol.*, 129(5):1000–1011, May 1989.
- [32] Szirmay-Kalos Laszlo, Gyorgy Antal, and Ferenc Csonka. *Haromdimenzios grafika, animacio es jatekfejlesztés*. ComputerBooks, Budapest, Hungary, 2003.
- [33] Michael Felsberg, Per-Erik Forssén, and Hanno Scharf. Channel smoothing: Efficient robust smoothing of low-level signal features. *IEEE transactions on pattern analysis and machine intelligence*, 28:209–22, 03 2006.
- [34] Cc by-sa 2.0 licence. <https://creativecommons.org/licenses/by-sa/2.0/>. Accessed: 2020-10-28.
- [35] Jorge Barbosa, Bruno Figueiredo, Nuno Bettencourt, and Joao Tavares. Towards automatic quantification of the epicardial fat in non-contrasted ct images. *Computer methods in biomechanics and biomedical engineering*, 14:905–14, 03 2011.
- [36] C. Pinter, A. Lasso, A. Wang, D. Jaffray, and G. Fichtinger. Slicerrt – radiation therapy research toolkit for 3d slicer. *Med. Phys.*, 39(10):6332–6338, 2012.
- [37] Les Piegl and Wayne Tiller. *The NURBS Book (2nd Ed.)*. Springer-Verlag, Berlin, Heidelberg, 1997.
- [38] Xiao-Diao Chen, Jun-Hai Yong, Guozhao Wang, Jean-Claude Paul, and Gang Xu. Computing the minimum distance between a point and a nurbs curve. *Computer-Aided Design*, pages 1051–1054, 10 2008.
- [39] Tamás Umenhoffer, Márton Tóth, Ágota Kacsó, László Szécsi, Ákos Szlávecz, Péter Somogyi, László Szilágyi, Anikó Kubovje, Tamás Szerafin, László Szirmay-Kalos, et al. Modeling and simulation framework of aortic valve for hemodynamic evaluation of aortic root replacement surgery outcomes. *IFAC-PapersOnLine*, 51(27):258–263, 2018.